Chapter 6

DISCUSSION

6.1 OXIDE OVERLAYER CHARACTERIZATION

6.1.1 Overlayer Coverage and Structure

The AES uptake plots of Figs. 5.5 and 5.13 reveal that both alumina and titania overlayers develop on the rhodium surface through the Stranski-Krastanov growth behavior, *i.e.*, growth of a two-dimensional monolayer followed by three-dimensional growth at higher coverages. Although deposited metals do not usually wet oxide substrates, in the reverse system, an oxide may be expected to spread over a metal surface. This is a result of the higher surface energy of exposed metal relative to the oxide [72], which in turn, leads to significant metal/metal oxide interaction. For oxide-supported metals, if the interaction is particularly strong, such as between titania and Group VIII metals, it may lead to the migration of oxide species from the support onto the surface of the metal particles. Once the free metal surface is covered, the driving force for layered growth is eliminated and minimization of surface area becomes the overriding criterion.

The degree of attenuation of the rhodium substrate signal at monolayer coverage was 0.45 for AlO_x/Rh and 0.34 for TiO_x/Rh. Metal-on-metal growth studies, though, show typical attenuation factors of 0.5–0.6 for 300–400 eV electrons (see Table 2.1). The larger attenuation for an oxide monolayer may be attributed to a more complex structure to the mono-

layer. Specifically, the two-component monolayer may likely exhibit a three-dimensional morphology which leads to a thicker "monolayer" than expected in a conventional one-component overlayer. For similar atomic densities, a metal oxide monolayer may then attenuate the substrate signal more than a metal monolayer due to the greater number of atoms covering the substrate.

Further information regarding the morphology of the oxide overlayers is difficult to obtain and has not been pursued in this study. Low energy electron diffraction (LEED) of the oxides on rhodium single crystals may provide information on the location of overlayer species relative to the substrate atoms if the metal oxide occupies positions at regular intervals on the substrate surface lattice. The width of LEED substrate spots may indicate the size of uncovered Rh domains and hence, the dispersion of the metal oxide on the surface. The application of scanning tunneling microscopy (STM) to this system would also provide information about the dispersion of metal oxide overlayers.

Determination of the relative positions of the metal and oxygen in the overlayer is not possible with the techniques on hand and would require techniques sensitive to M–O bond lengths and bond angles on the surface (HREELS, SEXAFS, *etc.*). However, if a distribution of bond lengths and orientations exists, even these techniques would prove ineffective. Perhaps the only plausible picture of the oxide overlayers at this level of understanding would be an extrapolation of the bulk morphologies. Examples of these for alumina [137] and titania [138,139] are shown in Fig. 6.1. The extent of distortion from these structures will depend on such factors as the degree of interaction (of both metal and oxygen) with the substrate, the preferred oxide orientation, substrate surface topology, and overlayer preparation conditions.

Attempts to clarify the oxide overlayer structures must be left to future investigations. Further discussion of the morphologies will be restricted to the nature of the metal/metal oxide interface at the periphery of oxide islands.

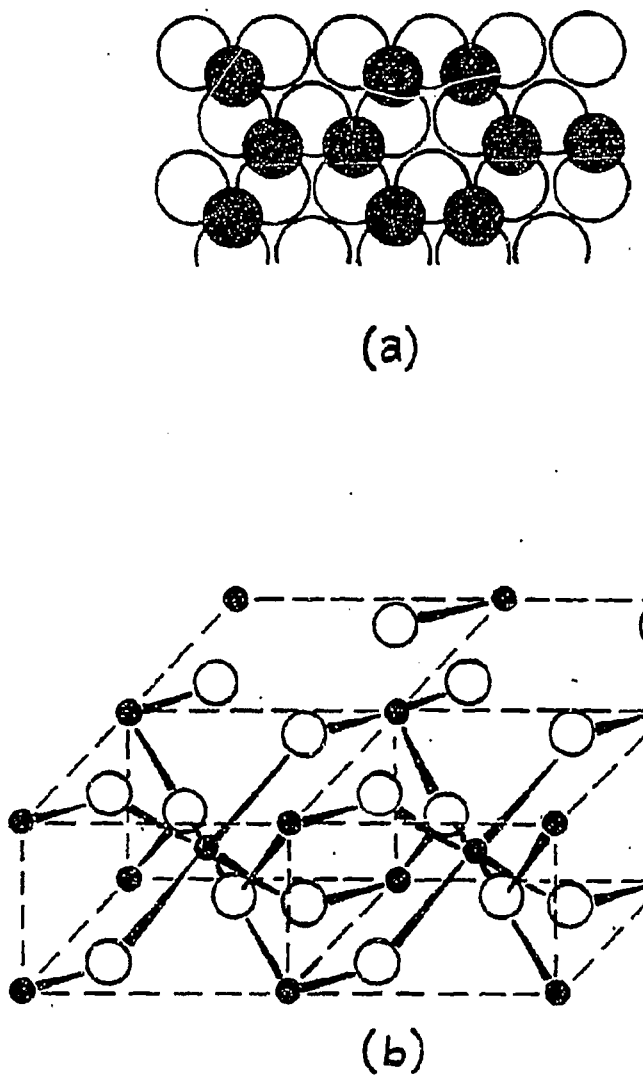

Figure 6.1: The bulk structures of (a) α-Al_2O_3 [137] and (b) TiO_2 (rutile) [138,139].

6.1.2 Overlayer Stoichiometry

Although overlayer morphological identification is not feasible with the available techniques, the oxide can be characterized in terms of the oxygen-to-metal ratio with AES and XPS. The comparison by AES of the oxide overlayers prepared in this study with bulk alumina and titania samples demonstrates the nearly-complete stoichiometry of the oxide overlayers. These observations are reinforced by XPS analyses showing the aluminum in the 3+ oxidation state and titanium predominantly in the 4+ state.

The differences in the effects of the aluminum and titanium oxides on the chemisorption and catalytic properties of rhodium can be related to their relative ease of reduction. While no reduction of the Al^{3+} by CO titration occurs, treatment in 50 torr hydrogen at 753 K induces reduction of no more than 10% of the Al^{3+} to Al^{0}. No intermediate cation states are thermodynamically stable. The inertness of the alumina overlayer to reducing conditions parallels the trends in Figs. 5.8 and 5.9 where alumina appears to only block CO chemisorption and hydrogenation sites in proportion to the coverage. Thus alumina acts as an inert contaminant on the surface of rhodium.

By comparison, reduction of titania is facile provided there is an adequate supply of a reducing agent on the surface. The treatment of titania on gold in a reducing atmosphere fails to produce any Ti^{3+} features in the XPS spectrum (Fig. 5.17) while conversion of more than 60% of the Ti^{4+} to Ti^{3+} is possible for titania on rhodium (Fig. 5.16). Clearly, reduction by gas-phase hydrogen does not take place. However, even exposure to CO followed by heating produces a significant quantity of Ti^{3+} in the rhodium-supported overlayer. Reduction of the titanium to the 2+ oxidation state can be accomplished by annealing sufficiently to cause diffusion of the oxide into the substrate.

It is also evident from Figure 5.24 that the process of overlayer reduction with H_2 is rapid, reaching the final state of reduction in less than 30 seconds at 753 K. The reduction may even be carried in the UHV chamber if desired.

Operation of the AES electron gun has also been observed to reduce surface titania as

evidenced by the AES O/Ti ratio. Though reduction to only ~TiO has been seen, other authors have noted more extreme oxygen removal upon impingement by an AES electron beam [64].

The process of reducing titania in the aforementioned examples is facilitated by the existence of Magnelli phases of composition Ti_nO_{2n-1}. The energetics of partial reduction to these suboxides are not prohibitively difficult—unlike complete reduction to Ti metal. Another factor which can aid titania reduction is the possible formation of Brewer–Engels-type alloys between the titanium and rhodium. The stability of this interaction provides an additional driving force for the removal of oxygen from the titania overlayer. No direct evidence for this interaction is provided by the results presented in this study, but, as will be seen later, the CO chemisorption results suggest that after H_2 reduction, redispersion of TiO_x islands on the rhodium surface occurs, increasing the amount of TiO_x–Rh interface.

Figs. 5.20 and 5.22 show increases in the Ti^{3+} and –OH percentages in the titania overlayer as lower coverages are reached. Since the perimeter-to-area ratio of the overlayer also rises with lower coverages, it appears that the much of the Ti^{3+} and –OH species reside at the periphery of titania islands. The higher degree of Ti^{3+} formation seen after H_2 reduction, as compared with after CO titration, reflects the greater ease of breaking Ti–O bonds at the island periphery. In the case of the –OH percentage in the overlayer, there is little dependence on pretreatment conditions. The severing of Ti–O bonds can be accomplished by the reduction of hydroxyl groups at the island perimeter to form water or by reduction of Ti–O–Ti to Ti–OH. These two schemes predict changes in opposite directions for the –OH percentage with pretreatment conditions. Taken together, they may cancel resulting in the observed negligible dependence on pretreatment conditions.

6.2 CO CHEMISORPTION

6.2.1 The Suppression of CO Chemisorption on Rhodium by Oxide Overlayers

Comparison of the coverage dependence of CO chemisorption on the AlO_x/Rh and TiO_x/Rh surfaces reveals striking differences in the effects of these oxide overlayers. Alumina was found to inhibit CO chemisorption in direct proportion to its coverage suggesting that alumina is present on the surface as an inert contaminant. In contrast, titania overlayers exhibit a further suppression of CO chemisorption capacity beyond that expected from blocking Rh sites underneath. It is emphasized that the coverages for these two oxides were determined by the same method (AES intensity–vs.–dosing time plots) and that the behavior exhibited in these determinations was very similar.

The additional suppression of CO chemisorption by titania is most likely to arise from effects at the TiO_x-Rh interface. Inhibition of CO chemisorption at Rh atoms along the perimeters of TiO_x islands is envisioned to occur by two means: (1) partial blocking of neighboring Rh atoms by TiO_x species residing in multiple-Rh atom sites (*e.g.*, bridge, 3-fold hollow) and (2) "bonding" between TiO_x species and neighboring Rh atoms, which in turn, would weaken the bonding of CO to those Rh sites. The implication of these modes is that CO chemisorption at Rh sites on the periphery of TiO_x islands may still occur, but with a reduced bond energy. The normal bond strength of CO on rhodium, as determined from first-order desorption kinetics (Eqn. 2.12) [116,117], is about 29 kcal/mole (Figs. 5.2 and 6.2). The absence of any new desorption features ascribable to CO on the "peripheral" rhodium sites at temperatures as low as 150 K indicates that if CO is bound at these sites, it would indeed be weakly bound, with a bond energy of no more than 8 kcal/mole.

A simple thought process eliminates the possibility that mode 1 above operates alone. If CO chemisorption is suppressed only by partial blocking of "peripheral" Rh sites by TiO_x species, comparison of the results for TiO_x and AlO_x overlayers suggests that there is much

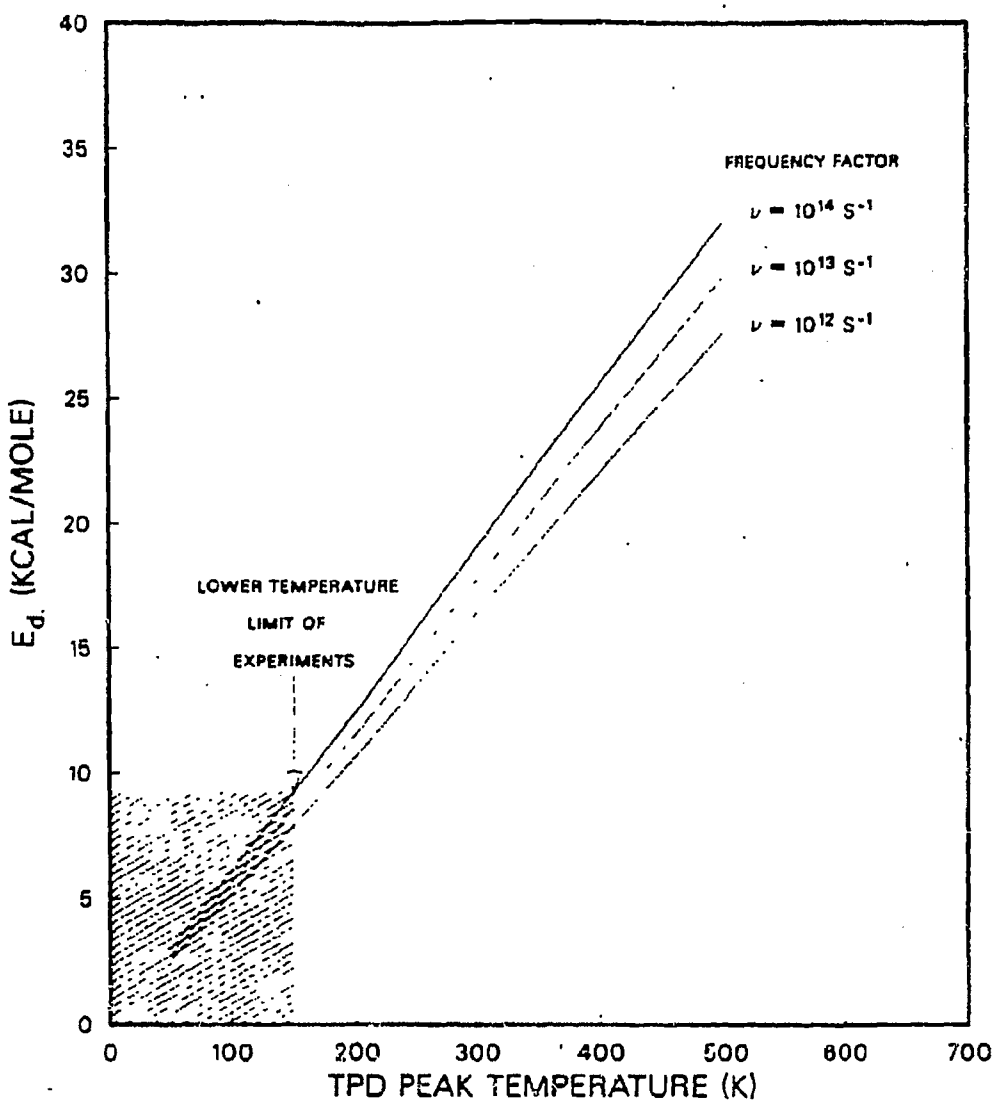

Figure 6.2: Desorption energy as a function of peak temperature for first-order desorption kinetics (from Eqn. 2.12).

more oxide perimeter for TiO_x than AlO_x (since AlO_x may have the same stereochemical effect on neighboring Rh atoms). This means that for identical coverages, TiO_x islands will be smaller than AlO_x islands, on the average, reflecting a higher dispersion. A higher dispersion for TiO_x must arise from a more substantial interaction between metal and metal oxide. The thermodynamically-favored Ti-Rh interaction described earlier provides the driving force for the greater dispersion of the TiO_x overlayer. This Ti-Rh interaction, though, leads to the second mode of suppression. Clearly, mode 1 cannot occur without mode 2.

Dwyer *et al.* detected a substantial concentration of Ti^{3+} species with XPS on a TiO_x-promoted Pt foil. Figure 5.20 shows that Ti^{3+} species are more prevalent at low TiO_x coverages where the perimeter-to-area ratio of TiO_x islands is higher. This trend reflects the stability of Ti^{3+} species at the oxide-metal interface. The density of states at the Fermi level of Rh atoms in the vicinity of the TiO_x-Rh interface may be influenced by these Ti^{3+} centers along the oxide island perimeter. Recent calculations by Feibelman and Hamann [50,51] have demonstrated that such perturbations can extend a few metal atom distances from the perturbing ion and could be responsible for changes in the chemisorptive properties of the affected metal atoms. Similar calculations by Joyner *et al.* [52] for the C/Ni system limit the local electronic effect to one atomic distance.

6.2.2 Modeling of CO Chemisorption on TiO_x/Rh

A description of the falloff in CO chemisorption capacity with TiO_x coverage can be provided from a model incorporating the ideas presented above. It is assumed that TiO_x islands nucleate at defect sites on the Rh surface and that the Rh sites covered by the islands, as well as those within m Rh–Rh bond distances (2.69 Å) of an island perimeter, are no longer available for CO chemisorption (at temperatures above 150 K). Rhodium sites affected by nearby Ti^{3+} centers are depicted in Fig. 6.3.

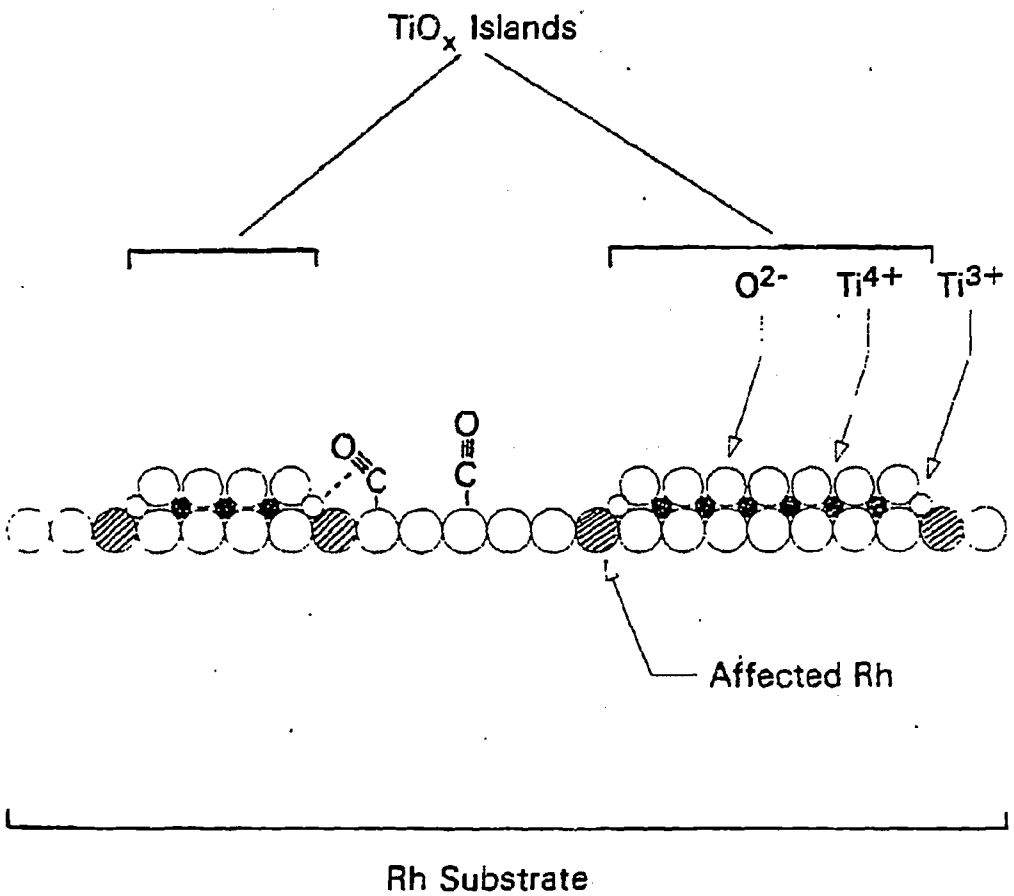

Figure 6.3: Schematic model for titania overlayers on rhodium.

Two approaches were taken to determine the number of Rh sites affected by nearby TiO_x species: one in terms of a mathematical expression and the other with a Monte Carlo simulation. The first requires uniform circular island growth around the nucleation sites and is essentially a continuum model. This leads to the following expression for the amount of CO that can be adsorbed at a given TiO_x coverage

$$A(\theta_{TiO_x})/A(0) = 1 - \pi[(\theta_{TiO_x}/\pi N)^{1/2} + m\delta]^2 N \qquad (6.1)$$

where $A(\theta_{TiO_x})$ is the CO coverage, N is the concentration of defect sites, and δ is the Rh-Rh bond distance (2.69 Å). This formulation accurately describes the data for CO adsorption over the range $0 \leq \theta_{TiO_x} \leq 0.3$ when, m=1 and N = 4.5 x 10^{13} cm^{-2} (Fig. 6.4). For $0.30 \leq \theta_{TiO_x} \leq \pi/4$, the overlap between excluded perimeter areas has to be taken into account to avoid counting it twice. By adopting a regular arrangement of TiO_x islands, the overlap can be calculated and subtracted from the excluded perimeter area. Equation 6.1 is then modified to

$$A(\theta_{TiO_x})/A(0) = 1 - R_0^2 N[\pi - 4\pi(\phi/360) + 4\sin(\phi/2)\cos(\phi/2)] \qquad (6.2)$$

where $\phi = 2\sin^{-1}[1 - 1/4R_0^2N]$

and $\pi[1/2 - \sqrt{N}m\delta]^2 \leq \theta \leq \pi/4$

for a square-lattice array of nucleation sites, the fit of the experimental data is extended by Eqn. 6.2 to nearly $\theta_{TiO_x} = 1.0$, as shown in Figure 6.4. The dependences on N and m in this model are shown in Figs. 6.5 and 6.6, respectively. It is also interesting to note that the density of TiO_x islands predicted by Eqs. 6.1–6.2 is roughly within an order of magnitude of that observed for Au, Pb, and Co islands nucleating on Pt(100), Cu(111), and Cu(100), respectively [134,135,136].

The Monte Carlo simulation of TiO_x growth was performed on a Commodore Model 8032 personal computer. A BASIC program was written to generate an array of points

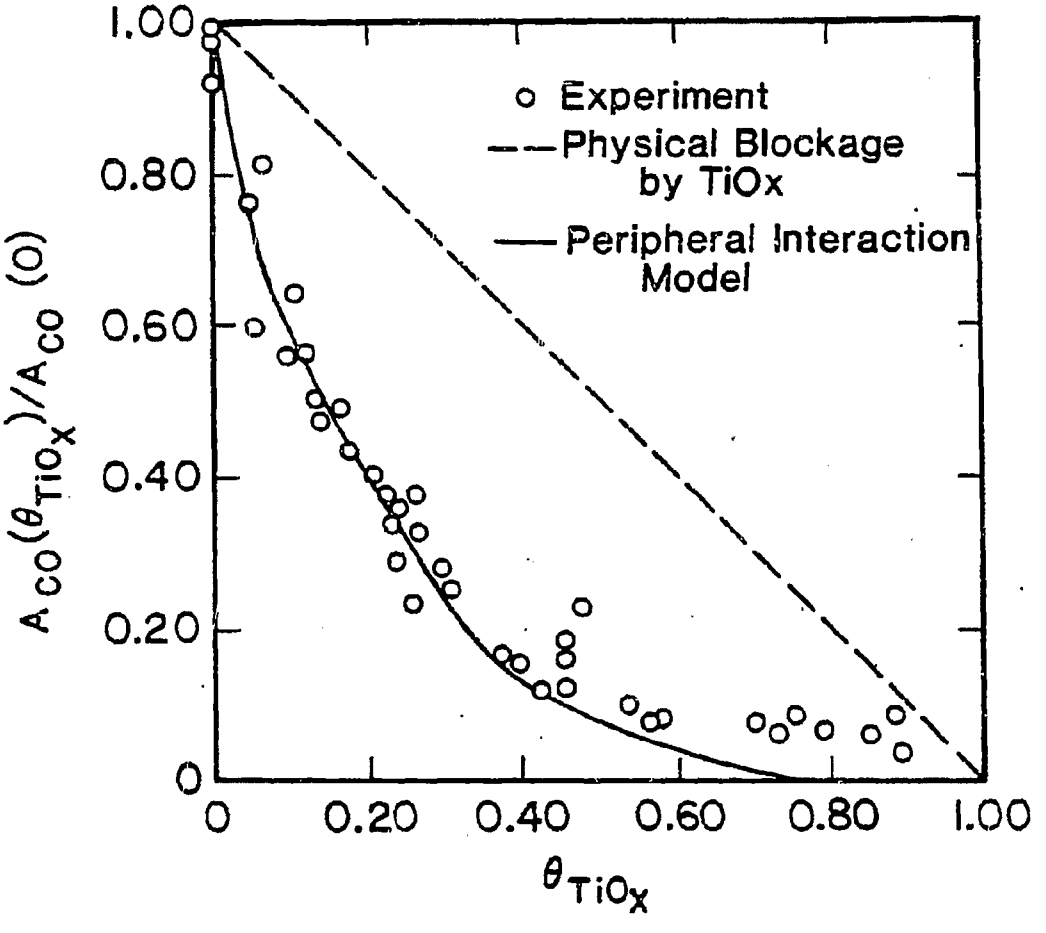

Figure 6.4: Comparison of island edge model and experiment for the dependence of CO coverage on TiO_x coverage. The solid line is given by Eqns. 6.1 and 6.2 for m = 1 and N = 4.5 x 10^{13} cm^{-2}.

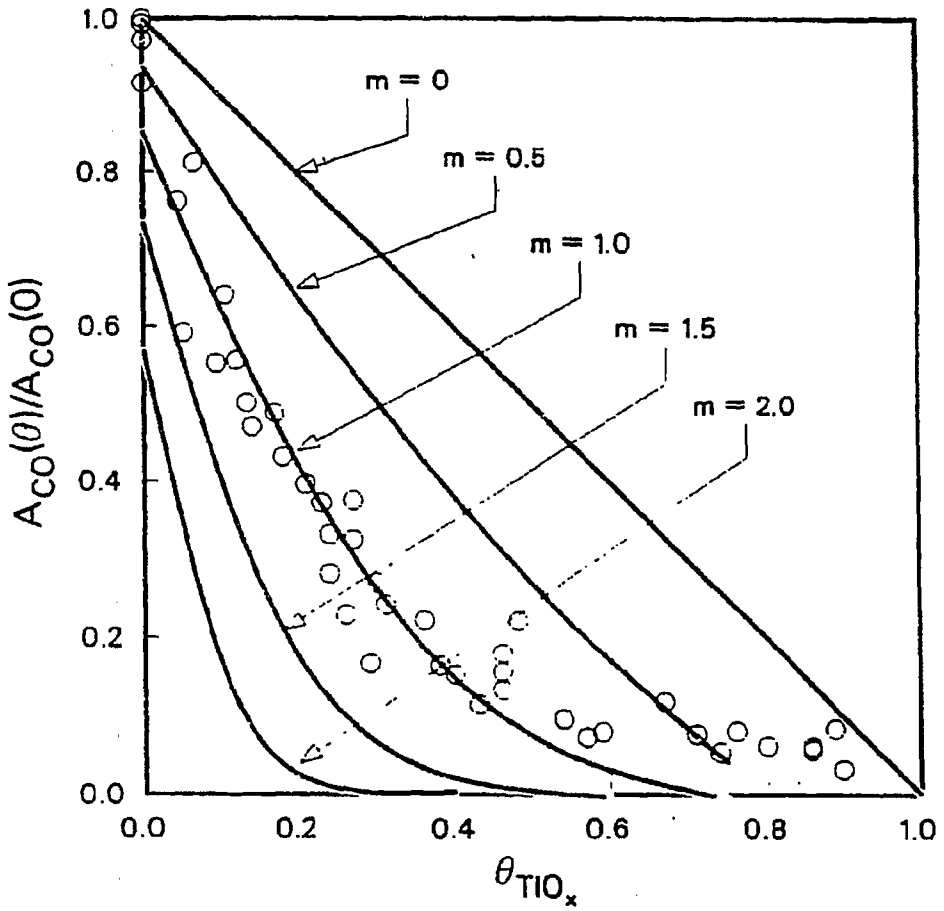

Figure 6.5: The effect of interaction distance on the predicted amount of CO chemisorbed on the TiO_x/Rh surface (Eqns. 6.1 and 6.2). The parameter m represents the number of Rh–Rh bond distances outward from the perimeter of TiO_x islands ($N = 4.5 \times 10^{13}$ cm^{-2}).

displayed on the visual memory representing the Rh surface. Nucleation sites were randomly chosen up to a pre-selected concentration. Island growth then proceeded by randomly blocking out points bordering the nucleation sites or along existing islands.. The number of rhodium atoms along the periphery of the TiO_x islands was then counted at various coverages. Although a square array was displayed, counting could be performed to simulate a hexagonal array by neglecting one pair of diagonally opposite corners as nearest neighbors. The code for this program appears in Appendix B.

Example visual displays appear in Fig. 6.7 showing clearly the irregular growth pattern

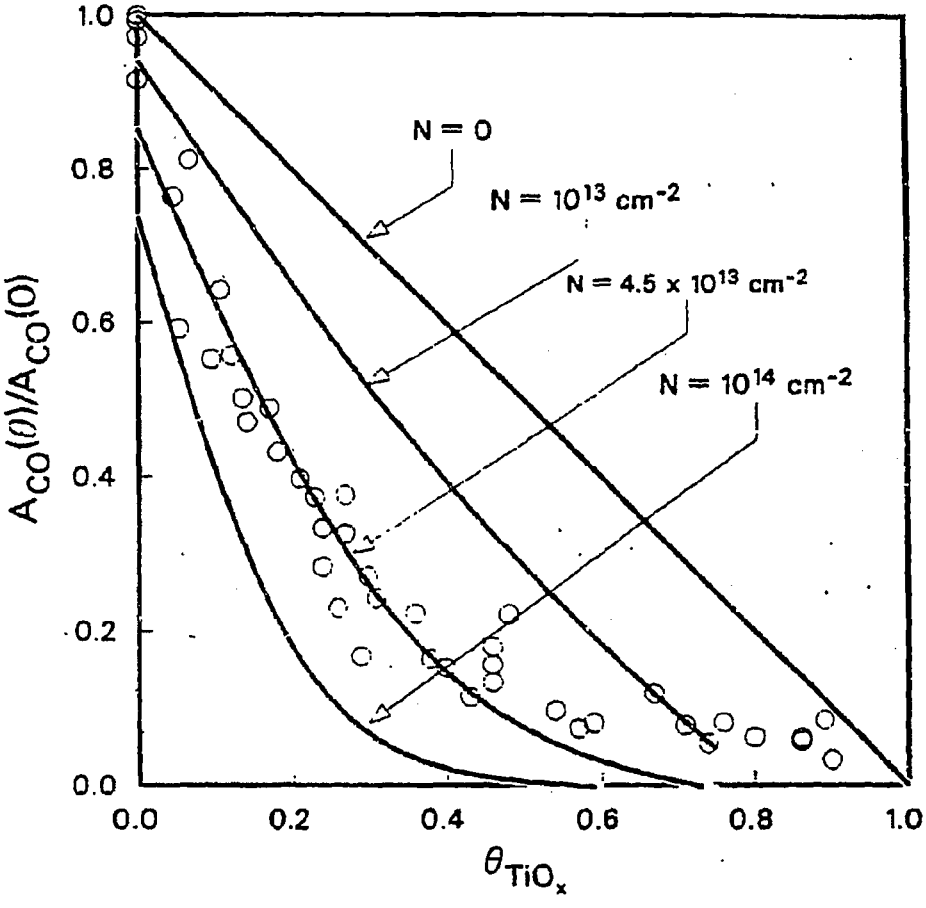

Figure 6.6: The effect of nucleation site density on the predicted amount of CO chemisorbed on the TiO_x/Rh surface (Eqns. 6.1 and 6.2). The parameter N represents the number of nucleation sites (m = 1).

of the islands which is believed to be more realistic than the assumptions associated with Eqn. 6.1. Figure 6.8 illustrates the expected CO chemisorption capacity as determined by the procedure just mentioned. For a 100 x 100 array and a nucleation site density of 4.5 x 10^{13} cm^{-2}, identical results are obtained to those from the uniform circular island growth model (compare Figs. 6.3 and 6.4). This indicates how even a simple depiction of the morphology of the surface, *i.e.*, uniformly-sized circular oxide islands, provides an adequate description on the macroscopic scale. The power of the Monte Carlo simulation lies in its flexibility and the ease of counting different types of sites while maintaining a closer link to

the actual surface morphology.

6.2.3 Effects of H_2 Reduction

At a fixed value of θ_{TiO_x}, we have observed that increasing the reduction temperature can result in a further suppression of the CO chemisorption capacity and a shift in CO TPD peak temperature to lower temperatures. These changes are accompanied by a decrease in the O/Ti ratio. The principal question now is whether the changes in CO chemisorption characteristics are due to the changes in the stoichiometry of the TiO_x layer, or to other causes. For example, one might imagine that with increasing reduction temperature, the number of TiO_x islands remains constant but that the magnitude of m associated with each island increases due to the decrease in the value of x. To fit the data for $T_{red} = 753$ K shown in Fig. 5.30, this interpretation would require m to increase from 1 to 1.25. The fractional value would indicate that only some of the next-nearest neighboring Rh atoms are affected. As an alternative, m may remain constant and the dispersion of the islands increase, thereby creating more perimeter. In this case, N would have to increase from 4.5 x 10^{13} cm^{-2} to 7.5 x 10^{13} cm^{-2} to fit the data.

Of the two alternatives presented above, the second seems more plausible than the first. From Fig. 5.36 it is evident that the reduction temperature influences the suppression of CO chemisorption only above a threshold temperature. It is also observed that the threshold temperature decreases with increasing TiO_x coverage. On the other hand, the O/Ti ratio of the overlayer decreases continually with increasing reduction temperature. What this suggests is that the reduction in O/Ti ratio is not directly responsible for the observed changes in CO chemisorption. Instead, the reduction in the O/Ti ratio facilitates the break-up of the TiO_x islands, once the O/Ti ratio has fallen below some critical value. Thus we contend that the suppression in CO chemisorption with increasing temperature, above the threshold value seen in Fig. 5.36, is the result of an increase in the number of

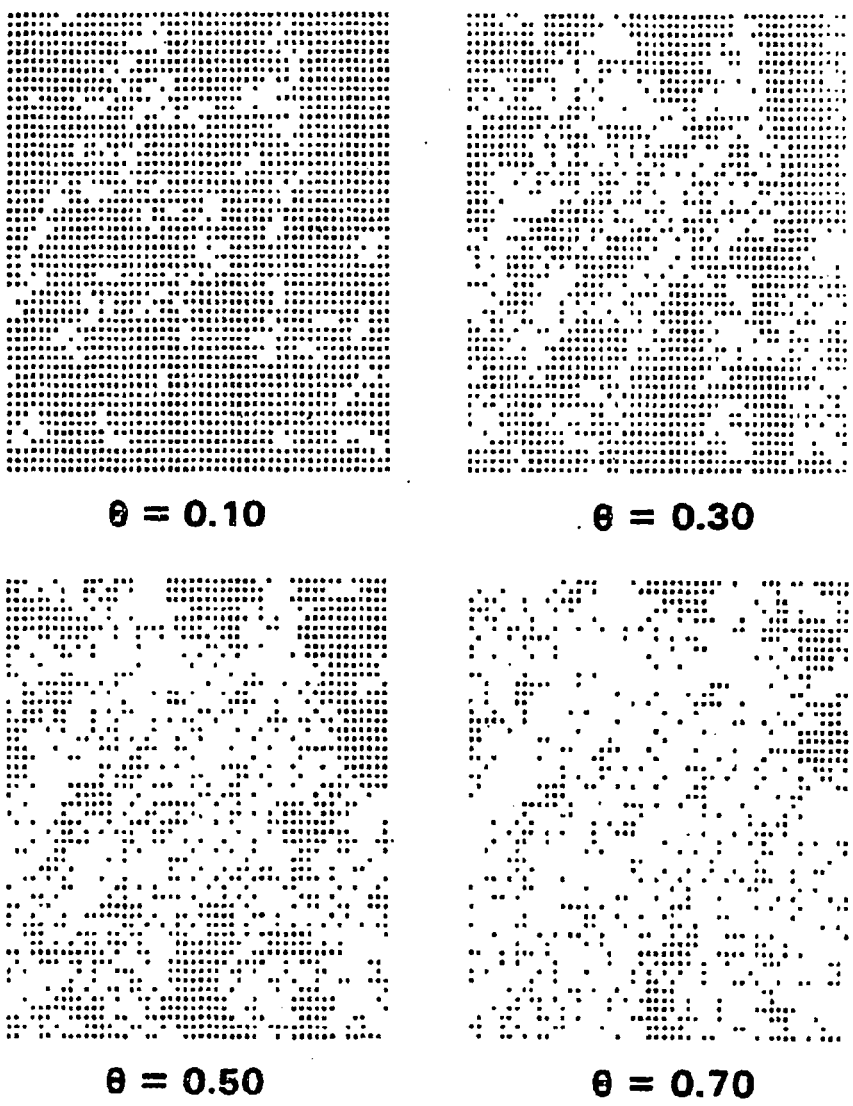

Figure 6.7: Computer simulation of titania island growth around fixed nucleation sites. Example visual displays for a 50 x 50 array are shown corresponding to coverages of (a) 0.10, (b) 0.30, (c) 0.50, and (d) 0.70 ML. A nucleation site density of 4.5 x 10^{13} cm$-$2 was employed.

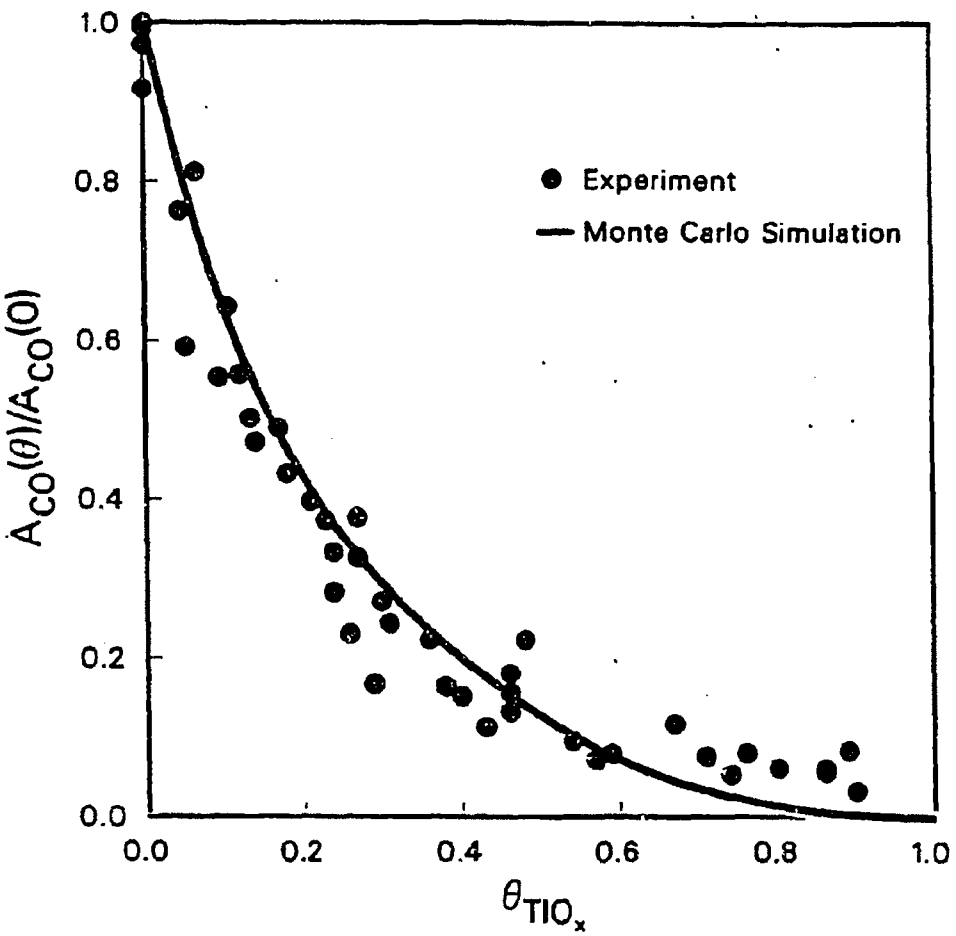

Figure 6.8: Comparison of the island edge model from a Monte Carlo simulation of TiO_x island growth with experiment data for the dependence of CO chemisorption on TiO_x coverage. All exposed Rh atoms were counted except for those adjacent to the perimeter of TiO_x islands. A nucleation site density of 4.5×10^{13} cm^{-2} was employed.

TiO_x islands and hence the perimeter area surrounding the islands.

6.3 CO HYDROGENATION

6.3.1 Reaction over AlO_x/Rh

It has already been noted that the presence of alumina overlayers results in the suppression of CO chemisorption on rhodium in direct proportion to the coverage. The same behavior is exhibited for CO hydrogenation on AlO_x/Rh indicating that alumina only physically blocks active sites for this reaction. The kinetic parameters and selectivity of this system are identical to those of the clean rhodium surface and agree well with those found for Al_2O_3-supported rhodium (see Table 6.1).

The degree of deactivation after one hour of reaction was largely independent of AlO_x coverage, averaging at roughly 80% of the initial activity. Also, no additional carbon was deposited on the surface in the presence of alumina. Clearly, alumina has no effect on the kinetics or deactivation of CO hydrogenation on rhodium.

6.3.2 Methane Formation over TiO_x/Rh

As indicated in Figure 5.38, a clear enhancement in methanation activity occurs for TiO_x coverages under 0.3 ML while at higher coverages, the rate diminishes gradually to a level well below that for clean Rh. This behavior was also observed by Chung *et al.* [88] for TiO_x deposited on a Ni(111) surface. Increases in activity of Pt foil [69], Pt-black [60], SiO_2-supported Pd [140], and SiO_2-supported Rh [141] have been found upon promotion with TiO_x.

It is apparent from Figs. 5.39 to 5.41 that at TiO_x coverages comparable to those where

Table 6.1: KINETICS FOR CO HYDROGENATION

LOADING (wt% Rh)	T (K)	H_2:CO	P_{tot} (atm)	$N^a_{CH_4}$ (x 10^3)	E^b_A	n (H_2)	m (CO)	SELECTIVITY x_{C_1}	x_{C_2}	x_{C_3}	Ref.
Rhodium											
—	573	3:1	0.9	150	24			0.89	0.09	0.03	[123]
—	573	2:1	6	260	25	1.0	-1.0	0.95	0.04	0.01	[122]
—	**553**	**2:1**	**1**	**37**	**24.4**	**1.0**	**-1.0**	**0.90**	**0.09**	**0.01**	*
Al_2O_3—Rhodium											
1	538	3:1	1	13	24.0	1.04	-0.20	0.89	0.09	0.02	[127]
1	548	3:1	1	11	24.0	0.90	-0.42	0.85	0.03	0.03	[142]
2.3	513	20:3	1	3.6	23.7			0.93	0.05	0	[143]
0.35	543	1:1	1	0.21				0.87	0.06	0.04	[144]
[c]	**553**	**2:1**	**1**	**11**	**24.7**	**1.1**	**-0.6**	**0.90**	**0.09**	**0.01**	*
TiO_2—Rhodium											
2	538			~11	33.2	1.7	-0.10				[13]
1	548	3:1	1	62	18.3	0.75	-0.88	0.75	0.04	0.03	[127]
7.8	573	3:1	1	5.4	36.2			0.77	0.03	0.04	[145]
3	573	1:2	10	0.22	41.5			0.50	0.32		[146]
[d]	**553**	**2:1**	**1**	**72**	**19.0**	**2.4**	**-0.3**	**0.67**	**0.22**	**0.11**	*

*This work

[a] Turnover frequency (molecules/site-s)

[b] Activation energy (kcal/mole)

[c] ~0.4 ML AlO_x/Rh

[d] ~0.2 ML TiO_x/Rh

R_{CH_4} reaches a maximum, the value of E_A is smaller, and the values of m and n are larger compared to the values of these parameters for clean Rh. A reduction in E_A has also been reported by Demmin *et al.* [69] for a TiO_x-promoted Pt foil and by Rieck and Bell [140] for TiO_x-promoted Pd/SiO_2. A sharp increase in hydrogen order was also observed by Vannice [13] for TiO_2-supported Rh in comparison with Al_2O_3-supported Rh, while only a slight change in the CO partial pressure dependence was found (see Table 6.1).

The influence of TiO_x on the CO hydrogenation activity of Group VIII metals has been attributed to Ti^{3+} ions present at the perimeter of small TiO_x islands decorating the metal surface [14,24,147,148,149,150,151,152]. For a TiO_x-promoted Pt foil, Dwyer *et al.* [67] detected a substantial concentration of Ti^{3+} species with x-ray photoelectron spectroscopy. XPS studies for TiO_x on Rh presented earlier have shown that the percentage of Ti^{3+} in the formed by either CO or H_2 reduction increases with lower TiO_x coverage. Since the perimeter-to-area ratio of overlayer islands also rises with lower TiO_x coverages, these results suggest that Ti-O bonds near the periphery of TiO_x islands are more prone to attack by reducing agents chemisorbed on the Rh metal. The oxygen deficient Ti^{3+} species along the oxide island periphery may then interact with the oxygen end of CO adsorbed on near-by metal sites, as shown in Fig. 6.9. When CO is adsorbed on Rh sites adjacent to the Rh-Ti boundary, the C-O bond is long enough for the oxygen to reach the Ti^{3+} ion. The acid-base interaction between CO and the oxophilic Ti^{3+} should enhance the dissociation of CO—an essential step in the formation of methane.

To explain the observed methanation rate dependence on TiO_x coverage, we can propose that an ensemble of Ti^{3+} and Rh sites near the periphery of the islands are the active sites where an enhancement in rate occurs. The simplest ensemble that can be considered would include a single Rh site at the periphery. To determine the number of Rh atoms at the titania island periphery, the Monte Carlo simulation of TiO_x island growth around fixed nucleation sites was employed with the nucleation site density determined in the CO chemisorption modeling (4.5×10^{13} cm^{-2}). Counting the number of these "peripheral" rhodium sites by use of the Monte Carlo simulation produces a function reaching a maximum at $\theta_{TiO_x} \approx$

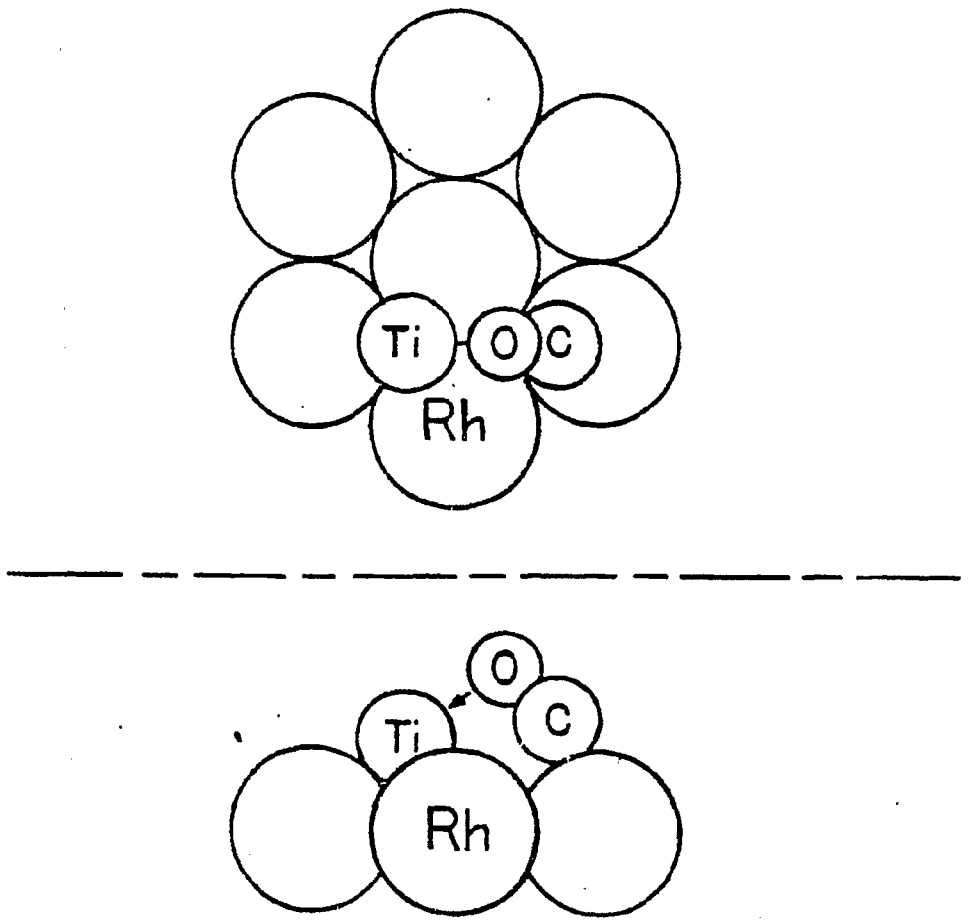

Figure 6.9: A possible configuration for the bonding of CO between peripheral Ti^{3+} sites and the Rh substrate.

0.35 ML, corresponding to the maximum chemisorption suppression at low pressures (Fig. 6.10). Neither the position of the maximum nor the shape of the curve agree with the trend of the experimental data.

A model which does give agreement with the observed trends is one in which a site pair consisting of a "peripheral" Rh site and an adjacent, non-"peripheral" Rh site has an intrinsically higher methanation activity. If it is assumed that the contribution of these peripheral site pairs to the total methanation rate is proportional to the product of the surface concentrations of each constituent site, then the total methanation rate in this model becomes

$$R_{CH_4} = S_T[n_o r_o + (\frac{n_p}{n_T})(\frac{n_{p'}}{n_T})r_{pp'}] \tag{6.3}$$

where r_o and $r_{pp'}$ represent the intrinsic methanation rates per unit catalyst area for the Rh sites unaffected by TiO_x and the highly active site pairs near the perimeter of the TiO_x islands, respectively. The numbers of each type of site present—exposed, "peripheral", adjacent to "peripheral", and the total—are given by n_o, n_p, $n_{p'}$, and n_T, respectively.

The number densities of the various types of site at various TiO_x coverages were determined through use of the Monte Carlo simulation. The values of n_o, n_p, and $n_{p'}$ were combined with the experimentally observed reaction rate for clean Rh, r_o, in Eqn. 6.3 to yield the total reaction rate as a function of coverage. The value of $r_{pp'}$ was chosen so that the maximum value of the predicted rate agrees with the maximum in the observed methanation rate. For this condition to be met, $r_{pp'}/r_o = 43$. The dependence of the calculated rate on the TiO_x coverage, described by Eqn. 6.3, is shown in Fig. 6.11 (solid curve), along with the experimental points presented in Fig. 5.38, for comparison. Good agreement is seen between the location of the predicted rate maximum and that of the experimental data. The width of the calculated peak, though, is broader than that exhibited by the data.

Another feature of this model is that it accounts for the extrema in kinetic parameters observed in Figs. 5.41 to 5.43. At low coverages ($\leq$ 0.3 ML), the rate is dominated by

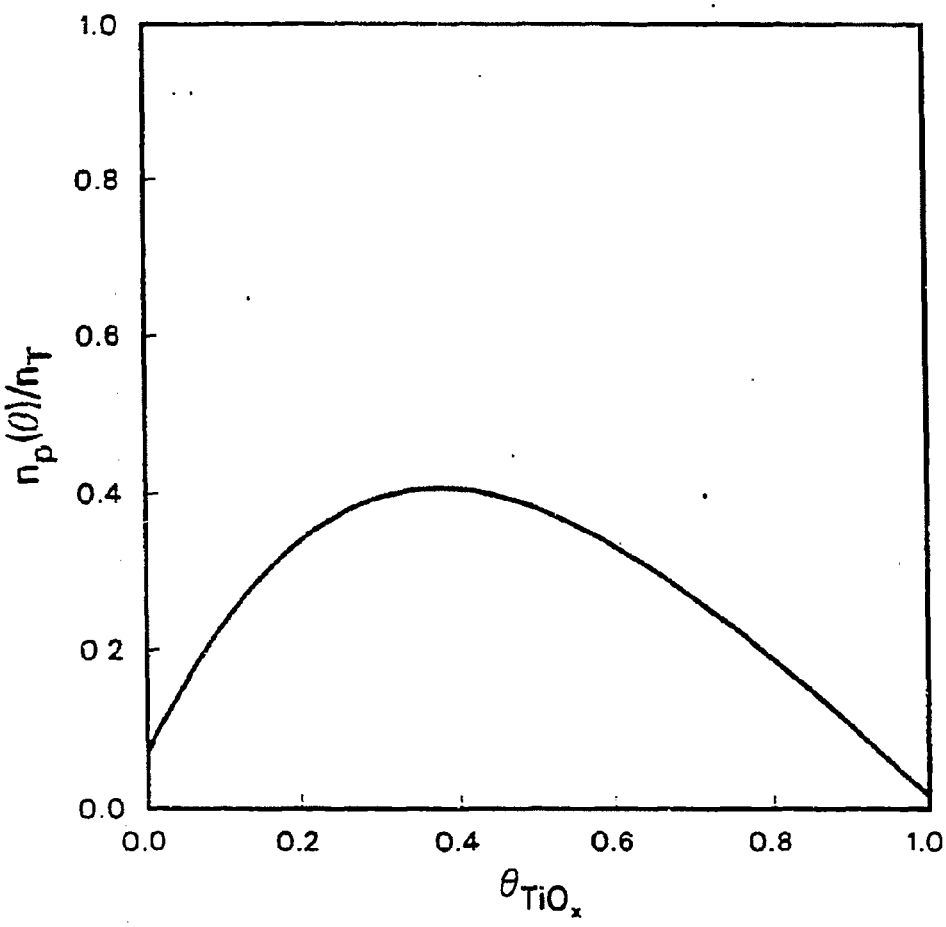

Figure 6.10: Amount of "peripheral" Rh sites as a function of TiO_x coverage based on a model in which CO chemisorption (at room temperature) is excluded at these sites (determined by subtracting the curve found in Fig. 5.30 (non-reduced) from the total amount of exposed Rh atoms.

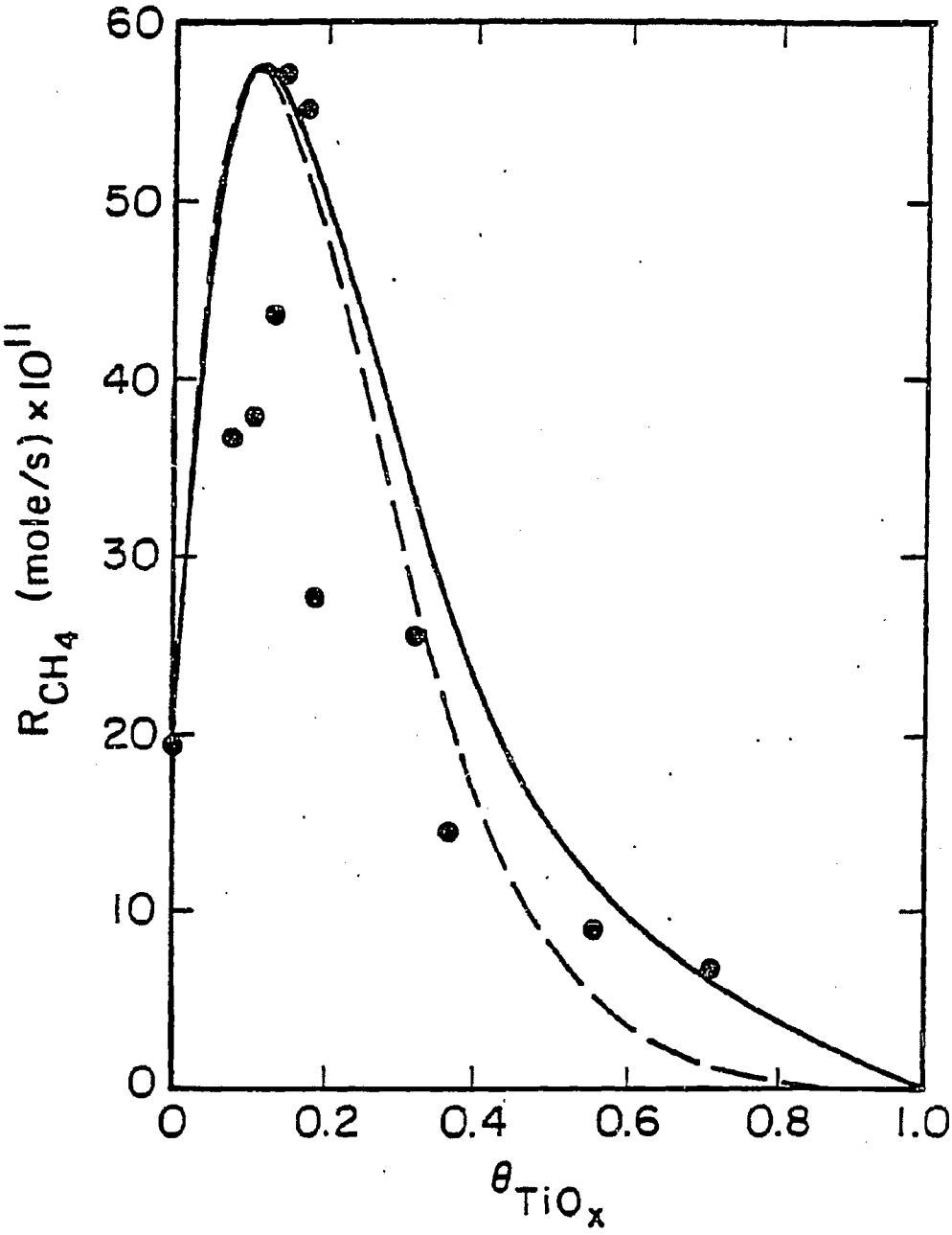

Figure 6.11: A comparison between the predicted methanation rate and the experimental data (●) as a function of TiO_x coverage. Solid curve— peripheral Rh sites active for both the Ti^{3+}-assisted reaction pathway and the normal reaction pathway. Dashed curve—peripheral Rh sites active only in the Ti^{3+}-assisted pathway.

the reaction occurring at the TiO_x/Rh interface, as reflected by the changes in activation energy and partial pressure dependences. At higher coverages, this contribution diminishes rapidly until kinetics typifying CO hydrogenation on clean Rh dominate.

At coverages approaching one monolayer, virtually all exposed, surface Rh atoms border TiO_x islands. These Rh sites may catalyze CO hydrogenation either through the mechanism normally occurring on Rh metal or through the Ti^{3+}-assisted pathway, depending on the prevalence of Ti^{3+} species at the metal/oxide interface under reaction conditions. The number of sites, n_o, catalyzing the reaction through the normal CO hydrogenation mechanism on bare Rh is therefore taken to be the total number of exposed Rh atoms.

The quantity, n_o, can be taken as the number of Rh atoms that could chemisorb CO at low pressures. The plot of predicted rate versus TiO_x in this case is depicted by the dashed curve in Fig. 6.11. However, with n_o defined in this manner, the model does not predict the extrema in kinetic parameters of Figs. 5.41 to 5.43.

Through bonding with the oxygen in CO, Ti^{3+} is oxidized to the +4 oxidation state. Regeneration of the Ti^{3+} site must occur for this reaction pathway to be followed again. One scheme for the reduction of Ti^{4+} back to Ti^{3+} is given below

1. Ti^{4+}—O—M + H(a) $\rightleftharpoons$ Ti^{4+}—OH (M = Rh or Ti^{4+})
2. Ti^{4+}—OH + H(a) $\rightleftharpoons$ Ti^{3+} + H_2O

The high reaction order of 2.6 with respect to hydrogen in the Ti^{3+}-assisted reaction pathway suggests that five or six hydrogenation steps are crucial in determining the overall reaction rate; Reactions 1 and 2 comprise two of these steps. In contrast, for bare Rh, where CO dissociation is believed to be rate-determining, the first-order H_2 dependence suggests that only two hydrogenation steps are important. Consequently, changes in the abundance of hydrogen on the surface are expected to affect the Ti^{3+}-assisted methanation rate to a greater extent.

As higher TiO_x coverages are reached, there is a reduction in the number of exposed

non-"peripheral" sites relative to the number of "peripheral" Rh sites. Furthermore, the high dispersion of the oxide overlayer serves to break up Rh–Rh pairs necessary for the chemisorption and dissociation of molecular hydrogen. The supply of surface hydrogen decreases rapidly with coverage and the impact on the Ti^{3+}-assisted reaction pathway, where the H_2 partial pressure dependence is nearly cubic, is much greater than on the normal pathway, where the dependence is only linear. At the microscopic level, this means that at near-monolayer coverages, there is insufficient surface hydrogen to maintain the Ti^{3+}-assisted reaction rate and so the slower pathway, in which CO dissociation is rate-determining, is the principal contributant.

The absence of any effect from pre-reduction of the sample upon reaction rate, as observed in this study and others [17,22,24,38] may be related to the active role of Ti^{3+} species in CO hydrogenation. Whether pre-oxidized or pre-reduced, the oxidation state (and perhaps also the morphology) of the oxide overlayer may be determined by the reaction conditions, where both H_2 and H_2O are present. In particular, the percentage of Ti^{3+} after reaction was found to be only weakly dependent on the pretreatment conditions (Fig. 5.27).

4.2 Formation of C_{2+} Hydrocarbons

Comparison of Figs. 5.44 to 5.46 with Figs. 5.41 to 5.43 shows two principal patterns: (1) the kinetics of ethane formation are similar to those of methane formation and (2) the kinetics of ethylene and propylene formation are likewise similar. Significant differences are seen only in the case of the CO partial pressure dependence (*e.g.*, -1.0 order for CH_4 and +0.5 order for C_2H_4) and these can be attributed to the requirement of additional surface carbon to form large hydrocarbons. Of particular interest is the difference in hydrogen partial pressure dependences between paraffins and olefins. The methane and ethane hydrogen orders are between 1/2 and 1 greater than for ethylene and propylene. Similar behavior was noted by Dictor and Bell [153] for unsupported Fe and by Kellner and Bell [154] for Al_2O_3-supported Ru. In both of these studies, a difference in order of roughly 1/2 was seen

between paraffins and olefins.

6.3.3 Deactivation of the Catalyst

Figs. 5.11 and 5.47 showed a decay in activity after one hour of reaction as a function of oxide coverage. Clearly, the coverages where higher methanation rates occurred were accompanied by higher degrees of catalyst coking as evidenced by the normalized rates and the normalized AES carbon intensities as a function of TiO_x coverage. The carbon signal reaches a maximum of about 0.44, compared with 0.12 for AlO_x/Rh, and at a TiO_x coverage near the point where the amount of oxide periphery is expected to reach a maximum ($\approx$ 0.35 ML based on the chemisorption modeling). Thus it appears that the additional carbon is deposited at the TiO_x/Rh interface along the periphery of TiO_x islands.

6.4 ETHYLENE HYDROGENATION AND ETHANE HYDROGENOLYSIS

Titania overlayers have been shown to enhance the hydrogenation of CC over rhodium, but as is apparent from Figs. 5.49 and 5.51, do not increase the rates of ethylene hydrogenation or ethane hydrogenolysis several possible hydrogenation steps). Rather, the rates of the latter two reactions diminish more rapidly than does the amount of exposed Rh with TiO_x coverage. The trends appear similar to that of CO chemisorption capacity as a function of coverage, but for reasons discussed below, the possible occurrence of mass transfer effects precludes any strong quantitative connections between the reactions and CO chemisorption behavior.

Clearly, the presence of TiO_x on the surface does not translate into higher hydrogenation rates. No enhancement in the rates appears to occur at the TiO_x–Rh interface which

suggests the necessity of a functional group, such as a carbonyl, on a reactant molecule for an interaction with Ti^{3+} to take place. The suppression in activity in both reactions can be attributed to three effects: (1) the coverage of Rh sites by TiO_x, (2) the break-up of ensembles by TiO_x on which the hydrocarbon reaction takes place, and (3) the break-up of Rh-Rh pairs for the chemisorption and dissociation of molecular hydrogen (as in Section 6.3.2). The ensemble size necessary for ethane hydrogenolysis has been investigated by other authors [155] and their conclusions point to a cluster of <4 metal atoms. Similar results might be expected in the case of ethylene hydrogenation. The precise numbers of Rh atoms per ensemble in either reaction cannot be relied upon too heavily until they can be confirmed by alternative means.

Inspection of Figs. 5.50 and 5.52 reveals that surface TiO_x has no appreciable effect on the activation energies for these reactions. This is further evidence that TiO_x does not appear to take an active role in these reactions. However, the activation energy for ethylene hydrogenation is only about half of that observed for supported Rh catalysts [124,125] and the activation energy for ethane hydrogenolysis is only about one-third of reported values (T = 513 K) [30,133]. These low activation energies, which are independent of the presence of TiO_x, may be due to interphase mass transfer limitations. At lower hydrogenolysis temperatures, where the corresponding reaction rate was significantly reduced, a normal activation energy was obtained. A calculation of the expected mass transfer rate during reaction conditions indicates that this should only marginally be a problem. Yet mass transfer limitations appear to be the most likely explanation for both diminished activation energies. Further study of this problem is warranted.

The effect of mass transfer limitations on the rate versus TiO_x coverage plots of Figs. 5.49 and 5.51 would be to diminish the rate dependence with coverage. If interphase transport is much slower than the surface reaction rate, then the overall rate would be independent of TiO_x coverage and would appear as a horizontal line. For Figs. 5.49 and 5.51, the actual surface rates are expected to decline more steeply with coverage than as they actually appear. In the case of CO hydrogenation, the rate is more than 30 times less active

than the ethylene hydrogenation and ethane hydrogenolysis reactions and so mass transport considerations do not apply.

Chapter 7

CONCLUSIONS AND RECOMMENDATIONS

7.1 CONCLUSIONS—EXPERIMENTAL

Oxide overlayers ($\leq$3 ML) on rhodium foil have been prepared in ultra-high vacuum through deposition of aluminum or titanium with subsequent oxidation. The AlO_x/Rh and TiO_x/Rh surfaces were characterized in terms of the oxide growth and chemisorption properties with surface analytical tools (AES, XPS, TPD) and in terms of their catalytic properties.

Both alumina and titania overlayers develop through the Stranski-Krastanov mechanism, i.e., formation of a two-dimensional monolayer followed by three-dimensional growth. As prepared, the two oxide overlayers, AlO_x and TiO_y, were only slightly substoichiometric, with x = 2.8 and y = 1.9.

The similarities between the two oxide overlayers end at this point. *Whereas reduction of the alumina overlayer is difficult, reduction of the titania with H_2 or CO is facile.* At low TiO_x coverages, nearly 70% of the titanium is in the 3+ oxidation state following reduction in 50 torr H_2 at 753 K. Under similar conditions, titania deposited on a gold foil could not be reduced, suggesting the need for an active metal, such as Rh, to dissociate H_2.

Thermal desorption and catalytic results indicate that *alumina acts only as an inert*

contaminant on the rhodium surface, physically blocking sites active for CO chemisorption and CO hydrogenation. The CO chemisorption capacity of alumina on rhodium was found to decrease linearly with increasing alumina coverage. The same trend was observed for the methanation rate as a function of coverage with no changes in selectivity occurring (~90 mol% CH_4 for all coverages). Alumina appears to have no effect on the rate of deactivation as well as the amount of carbon deposited on the surface.

Titania overlayers were found to induce a sharp suppression in CO chemisorption which could only partly be attributed to site-blocking by the oxide. A further reduction in the CO chemisorpton capacity occurred upon hydrogen reduction at temperatures above ~520 K. While a downward shift in desorption temperature was noted for high TiO_x coverages or after hydrogen reduction, no new significant desorption ' 'res appeared, even at temperatures as low as 150 K.

A three-fold enhancement in CO hydrogenation activity occurred for a TiO_x coverage of 0.15 ML. This was accompanied by dramatic changes in the kinetic parameters, suggesting an alternative reaction pathway for Rh in the presence of TiO_x. In addition, there was an increase in selectivity toward ethylene and propylene. The presence of surface titania also led to a greater rate of deactivation and carbon deposition during reaction.

In contrast, *both the ethylene hydrogenation and ethane hydrogenolysis rates were substantially diminished by TiO_x on the surface.* Both activities were suppressed at least to the extent exhibited by CO chemisorption, but the actual amounts may be masked by mass transfer effects. The activation energies of these two reactions remained unchanged when TiO_x was added indicating that changes in mechanisms are unlikely. Comparison with the CO hydrogenation results suggests the need for a functional group, such as –C=O, for the Ti^{3+}-assisted reaction pathway to occur.

7.2 CONCLUSIONS—MODELING

The modification of the chemisorption and catalytic properties of Rh by TiO_x overlayers can

be attributed to processes occurring at the TiO_x/M interface at the TiO_x island periphery. In particular, XPS results point to the existence of Ti^{3+} sites along the periphery of TiO_x islands. These species may interact with neighboring Rh atoms, reducing the bond order of those Rh atoms, and thereby substantially weaken CO chemisorption. Under conditions for CO hydrogenation, these Ti^{3+} sites may interact with the oxygen of chemisorbed CO to enhance dissociation of the C–O bond and therefore the surface activity.

The suppression of CO chemisorption on a TiO_x/Rh surface has been successfully modeled by excluding CO chemisorption at Rh sites bordering as well as underneath TiO_x islands. The morphology of TiO_x species on the surface was simulated with two approaches: uniform circular islands grown around fixed nucleation sites and a Monte Carlo simulation of random island growth around randomly chosen nucleation sites. The number of Rh atoms bordering TiO_x islands can then be counted. Comparison of the results of either approach with the experimental data suggests a nucleation site density of 4.5×10^{13} cm^{-2} (a 2.8% site density). The high dispersion inferred from the nucleation site density probably reflects a high degree of Brewer-Engels-type alloying between the TiO_x species and the Rh.

Modeling of the methanation rate as a function of TiO_x coverage suggests a higher activity on two-site ensembles along the TiO_x island periphery. Whereas the Monte Carlo simulation (with the same dispersion as in the CO chemisorption modeling) yields a broad function with a maximum at 0.35 ML for a one-site ensemble, the two-site ensemble gives a sharper function reaching a peak at 0.10 ML. This agrees more closely with the experimental results. The model also allows for the return of the kinetic parameters at near-monolayer coverages to values typical of bare Rh. At the high TiO_x coverages, the supply of adsorbed hydrogen is inadequate to maintain Ti in the 3+ oxidation state and so the contribution from the Ti^{3+}-assisted reaction pathway is diminished.

7.3 RECOMMENDATIONS

While this work has demonstrated the importance of the titania/rhodium interface in CO chemisorption and hydrogenation, further exploration of metal oxide/metal systems is required to clarify the nature of the interactions taking place.

Structural information is vitally important. Knowledge concerning the positions and orientations of the overlayer atoms relative to the substrate could supply valuable information on the interaction between oxide overlayer and metal substrate and the participation of the metal oxide/metal interface in reactions. Although the determination of surface structures of this type are extremely difficult, the application of scanning tunneling microscopy (STM) and low energy electron diffraction (LEED) with single crystal substrates may provide a basis for understanding the overlayer structure relative to the substrate.

The effect of oxide overlayers on the chemisorption of other molecules should be investigated. Titania has already been shown to suppress CO chemisorption; chemisorption of other molecules, such as H_2 or NO, may be similarly affected. Perhaps some molecules may show no effect at all. Chemisorption on the oxide, for example by CO_2 or H_2O, may even be affected by the metal substrate. Finally, exploring the effect of oxide dispersion through the variation of adsorbate molecule size (H_2 vs. CO or C_3H_8 vs C_6H_{14}) may prove interesting.

By studying the reactions of hydrocarbons with –C=O groups on TiO_x/M surfaces, the role of "peripheral" Ti^{3+} in dissociation of the C–O bond may be investigated further. Other probe reactions include: the reduction of NO to N_2 by CO; CO + H_2 + C_2H_4 to form propanaldehyde; and reactions of hydrocarbons with other functional groups (*e.g.*, –COOH, –OH). Hydrocarbon hydrogenation and hydrogenolysis activities have already been shown to be suppressed by TiO_x on the surface. Perhaps these diminished activities can be related to the dispersion of the TiO_x overlayer.

Finally, *interactions between metal oxides and metals are not unique to the TiO_x/Rh system and other oxide/substrate systems should be studied.* Other suitable oxides include:

SiO_2, MnO_2, ZrO_2, V_2O_5, and La_2O_3. Some of these oxides may exhibit an interaction intermediate in strength compared with Al_2O_3 and TiO_2. Variation of the substrate is also possible and some of the likely candidates are: Ni, Ru, Fe, Pt, and Cu. Alloying between Pt and Ti makes the formation of a TiO_x overlayer extremely difficult and for this reason, a Pt substrate is not recommended. Also, the TiO_x/Ni and TiO_x/Pt systems have already been studied extensively in other research groups. Preliminary work with a Au substrate has been performed and may prove valuable when investigating the properties of the oxide overlayer.

Bibliography

[1] G.M. Schwab, J. Block, W. Müller, and D. Schultze, *Naturwissenschaftern*, **44**, 582 (1957).

[2] G.M. Schwab, J. Block, and D. Schultze, *Angew. Chem.*, **71**, 101 (1953).

[3] G.M. Schwab, "Advances in Catalysis," Vol. 27, p.1, Academic Press, New York, 1978.

[4] Z.G. Szabó, F. Solymosi, and I. Batta, *Z. Phys. Chem. N.F.*, **17**, 125 (1958).

[5] Z.G. Szabó, F. Solymosi, and I. Batta, *Z. Phys. Chem. N.F.*, **23**, 56 (1960).

[6] F. Solymosi, *Catal. Rev*, **1**, 233 (1967).

[7] R.F. Baddour and R.F. Deibert, *J. Phys. Chem.*, **70**, 2173 (1966).

[8] S.J. Tauster, S.C. Fung, and R.L. Garten, *J. Am. Chem. Soc.*, **100**, 170 (1978).

[9] S.J. Tauster, and S.C. Fung, *J. Catal*, **55**, 29 (1978).

[10] S.J. Tauster, S.C. Fung, R.T.K. Baker, and J.A. Horsley, *Science*, **211**, 1121 (1981).

[11] J.S. Smith, P.A. Thrower, and M.A. Vannie, *J. Catal.*, **68**, 270 (1981).

[12] P. Mériaudeau, O.H. Ellestad, M. Dufaux, and C. Naccache, *J. Catal.*, **75**, 243 (1982).

[13] M.A. Vannice, *J. Catal.*, **74**, 199 (1982).

[14] R. Burch and A.R. Flambard, *J. Catal.*, **78**, 389 (1982).

[15] J.M. Herrmann and P. Pichat, *J. Catal.*, **78**, 425 (1982).

[16] M.A. Vannice, C.C. Twu, and S.H. Moon, *J. Catal.*, **79**, 70 (1982).

[17] M.A. Vannice, C.C. Twu, and S.H. Moon, *J. Catal.*, **82**, 213 (1983).

[18] D.E. Resasco and G.L. Haller, *J. Phys. Chem.*, **88**, 4552 (1984).

[19] X.-Z. Jiang, T.F. Hayden, and J.A. Dumesic, *J. Catal.*, **83**, 168 (1983).

[20] C.H. Bartholomew and R.B. Pannell, *J. Catal.*, **65**, 390 (1980).

[21] S.-M. Fang and J.M. White, *J. Catal.*, **83**, 1 (1983).

[22] F. Solymosi, I. Tombácz, and M. Kocsis, *J. Catal.*, **75**, 78 (1982).

[23] R. Burch and A.R. Flambard, *J. Catal.*, **85**, 16 (1984).

[24] J.D. Bracey and R. Burch, *J. Catal.*, **86**, 384 (1984).

[25] V. Rives-Arnau and G. Munuera, *Appl. Surf. Sci.*, **6**, 122 (1980).

[26] R. Nakamura, S. Nakai, K. Sugiyama, and E. Echigoya, *Bull. Chem. Soc. Jpn.*, **54**, 1950 (1981).

[27] R. Nakamura, K. Yamagami, S. Nishiyama, H. Niiyama, and E. Echigoya, *Chem. Lett.*, 2, 275 (1981).

[28] N.K. Pande and A.T. Bell, *J. Catal.*, **98**, 7 (1986).

[29] D.E. Resasco and G.L. Haller, *J. Catal.*, **82**, 279 (1983).

[30] E.I. Ko and R.L. Garten, *J. Catal.*, **68**, 233 (1981).

[31] E.I. Ko and G. Marcelin, *J. Catal.*, **93**, 201 (1985).

[32] A. Sárkány and P. Tétényi, *React. Kinet. Catal. Lett.*, **12**, 297 (1979).

[33] D.J.C. Yates, W.F. Taylor, J.H. Sinfelt, *J. Am. Chem. Soc.*, **86**, 2996 (1964).

[34] L. Brewer, *Acta Met.*, **15**, 553 (1967).

[35] L. Brewer and P.R. Wengert, *Metall. Trans.*, **4**, 83 (1973).

[36] P.T. Meschter and W.L. Worrell, *Metall. Trans. A*, **7A**, 299 (1977).

[37] J.A. Horsley, *J. Am. Chem. Soc.*, **101**, 2870 (1979).

[38] S.R. Morris, R.B. Moyes, and P.B. Wells, in "Studies in Surface Science and Catalysis" (B. Imelik *et al.*, Eds.), Vol. 11, p.247, Elsevier, Amsterdam (1982).

[39] T. Huizinga and R. Prins, *J. Phys. Chem.*, **85**, 2158 (1981).

[40] B.A. Sexton, A.E. Hughes, and K. Foger, *J. Catal.*, **77**, 85 (1982).

[41] R.T.K. Baker, E.B. Prestridge, and L.L. Murrell, *J. Catal.*, **79**, 348 (1983).

[42] R.T.K. Baker, E.B. Prestridge, and L.L. Murrell, *J. Catal.*, **56**, 390 (1979).

[43] M.K. Bahl, S.C. Tsai, and Y.W. Chung, *Phys. Rev. B*, **21**(4), 1344 (1980).

[44] C.C. Kao, S.C. Tsai, M.K. Bahl, Y.W. Chung, and W.J. Lo, *Surf. Sci.*, **95**, 1 (1980).

[45] S.C. Fung, *J. Catal.*, **76**, 225 (1982).

[46] D.N. Belton, Y.-M. Sun, and J.M. White, *J. Phys. Chem.*, **88**, 1690 (1984).

[47] J.M. Herrmann, *J. Catal.*, **89**, 404 (1984).

[48] V. Ponec in "Studies in Surface Science and Catalysis" (B. Imelik *et al.*, Eds.), Vol. 11, p. 63, Elsevier, Amsterdam (1982).

[49] U. Bardi, G.A. Somorjai, and P.N. Ross, *J. Catal.*, **85**, 272 (1984).

[50] P.J. Feibelman and D.R. Hamann, *Phys. Rev. Lett.*, **52**, 61 (1984).

[51] P.J. Feibelman and D.R. Hamann, *Surf. Sci.*, **149**, 48 (1985).

[52] R.W. Joyner, J.B. Pendry, D.K. Saladin, and S.R. Tennison, *Surf. Sci.*, **138**, 84 (1984).

[53] J. Santos, J. Phillips, and J.A. Dumesic, *J. Catal.*, **81**, 147 (1983).

[54] P. Turlier, J.A. Dalmon, and B.A. Martin, in "Studies in Surface Science and Catalysis" (B. Imelik *et al.*, Eds.), Vol. 11, p. 203 (1982).

[55] H.R. Sadeghi and V.E. Henrich, *J. Catal.*, **87**, 279 (1984).

[56] S. Takatani and Y.-W. Chung, *J. Catal.*, **90**, 75 (1984).

[57] D.N. Belton, Y.-M. Sun, and J.M. White, *J. Phys. Chem.*, **88**, 5172 (1984).

[58] R.T.K. Baker, J.J. Chludzinski, and J.A. Dumesic, *J. Catal.*, **93**, 312 (1985).

[59] E.L. Kugler and R.L. Garten, U.S. Patent #4,273,724 (1981).

[60] D.J. Dwyer, J.L. Robbins, S.D. Cameron, N. Dudash, and J. Hardenbergh, *ACS Symposium Ser.*, No. 298, "Strong Metal Support Interaction" (R.T.K. Baker, S.J. Tauster, and J.A. Dumesic, Eds.), p. 21, 1986.

[61] N.K. Pande and A.T. Bell, *Appl. Catal.*, **20**, 109 (1986).

[62] G.B. Raupp and J.A. Dumesic, *J. Phys. Chem.*, **88**, 660 (1984).

[63] G.B. Raupp and J.A. Dumesic, *J. Catal.*, **95**, 587 (1985).

[64] C.S. Ko and R.J. Gorte, *J. Catal.*, **90**, 59 (1984).

[65] C.S. Ko and R.J. Gorte, *Surf. Sci.*, **161**, 597 (1985).

[66] C.S. Ko and R.J. Gorte, *Surf. Sci.*, **155**, 296 (1985).

[67] D.J. Dwyer, S.D. Cameron, and J. Gland, *Surf. Sci.*, **159**, 430 (1985).

[68] Y.-W. Chung, G. Xiong, and C.-C. Kao, *J. Catal.*, **85**, 237 (1984).

[69] R.A. Demmin, C.S. Ko, and R.J. Gorte, *J. Phys. Chem.*, **89**, 1151 (1985).

[70] R.A. Demmin and R.J. Gorte, *J. Catal.*, **98**, 577 (1986).

[71] D. Briggs and M.P. Seah, "Practical Surface Analysis by Auger and X-Ray Photoelectron Spectroscopy," John Wiley & Sons, 1983.

[72] G.A. Somorjai, "Chemistry in Two Dimensions," Cornell University Press, 1981.

[73] P.W. Palmberg, G.E. Riach, R.E. Weber, and N.C. MacDonald, "Handbook of Auger Electron Spectroscopy," Physical Electronics Industries, Eden Prairie, MN, 1972.

[74] R.W. Vook, *Inter. Metals Rev.*, **27**, 209 (1982).

[75] J.P. Biberian and G.A. Somorjai, *Surf. Sci.*, **2**, 352 (1979).

[76] E. Bauer, *Appl. Surf. Sci.*, **11/12**, 479 (1982).

[77] J.W.A. Sachtler, M.A. Van Hove, J.P. Biberian, and G.A. Somorjai, *Surf. Sci.*, **110**, 19 (1981).

[78] R.C. Yeates, Ph.D. Thesis, University of California, Berkeley, California, 1985.

[79] J.H. Ho and R.W. Vook, *J. Cryst. Growth*, **44**, 561 (1978).

[80] C. Binns and C. Norris, *Surf. Sci.*, **116**, 338 (1982).

[81] A. Sepulveda and G.E. Rhead, *Surf. Sci.*, **66**, 436 (1977).

[82] M.-G. Barthès and G.E. Rhead, *Surf. Sci.*, **80**, 421 (1979).

[83] C. Argile and G.E. Rhead, *Surf. Sci.*, **78**, 115 (1978).

[84] L. Gonzalez, Ph.D. Thesis, Universidad Autonoma de Madrid, 1982.

[85] G. Praline, N. Pacia, J.J. Ebrhardt, A. Cassuto, and J.P. Langeron, *Surf. Sci.*, **105**, 289 (1981).

[86] U. Bardi, G.A. Somorjai, and P.N. Ross, personal communication.

[87] P.W. Davies, M.A. Quinlan, and G.A. Somorjai, *Surf. Sci.*, **121**, 290 (1982).

[88] C. Argile and G.E. Rhead, *Surf. Sci.*, **78**, 125 (1978).

[89] H. Tokutaka, K. Nishimori, and K. Takashima, *Surf. Sci.*, **86**, 54 (1979).

[90] M.-G. Barthès and G.E. Rhead, *Surf. Sci.*, **85**, L211 (1979).

[91] K. Lewis and G.A. Somorjai, results to be published.

[92] G. Le Lay, M. Manneville, and J.J. Métois, *Surf. Sci.*, **123**, 117 (1982).

[93] R.A. Metzger and F.G. Allen, *Surf. Sci.*, **137**, 397 (1984).

[94] W. Kirstein, B. Krüger, and F. Thieme, *Surf. Sci.*, **176**, 505 (1986).

[95] L. Gonzalez, R. Miranda, M. Salmeron, J.A. Vergés, F. Ynduráin, *Phys. Rev. B*, **24**(6), 3245 (1981).

[96] D. Godbey and G.A. Somorjai, to be published.

[97] U. Gradmann and G. Waller, *Surf. Sci.*, **116**, 539 (1982).

[98] P.R. Davis, *Surf. Sci.*, **91**, 385 (1980).

[99] W. Schlenk and E. Bauer, *Surf. Sci.*, **93**, 9 (1980).

[100] Ch. Park, E. Bauer, and H. Poppa, *Surf. Sci.*, **154**, 371 (1985).

[101] D. Godbey and G.A. Somorjai, to be published.

[102] D.R. Strongin and G.A. Somorjai, to be published.

[103] U. Bardi, P.N. Ross, and G.A. Somorjai, *J. Vac. Sci. Technol. A*, **2**(1), 40 (1984).

[104] K. Christmann, G. Ertl, and H. Shimuzu, *J. Catal.*, **61**, 397 (1980).

[105] C. Harendt, K. Christmann, W. Hirschwald, and J.C. Vickerman, *Surf. Sci.*, **165**, 413 (1986).

[106] R. Siuda, *Surf. Sci.*, **123**, L667 (1982).

[107] A. Rolland, J. Bernardini, M.-G. Barthès-Labrousse, *Surf. Sci.*, **143**, 579 (1984).

[108] G.C. Smith, H.A. Padmore, and C. Norris, *Surf. Sci.*, **119**, L287 (1982).

[109] D.R. Strongin and G.A. Somorjai, unpublished results.

[110] S.R. Bare, D.R. Strongin, and G.A. Somorjai, *J. Phys. Chem.*, **90**, 4726 (1986).

[111] S. Nakanishi and T. Horiguchi, *Surf. Sci.*, **133**, 605 (1983).

[112] D.C. Jackson, T.E. Gallon, and A. Chambers, *Surf. Sci.*, **36**, 381 (1973).

[113] G. Ertl and J. Küppers, "Low Energy Electrons and Surface Chemistry," Verlag Chemie, 1974.

[114] C.D. Wagner, W.M. Riggs, L.E. Davis, J.F. Moulder, and G.E. Muilenberg (Editor), "Handbook of X-Ray Photoelectron Spectroscopy," Perkin-Elmer Corporation, Physical Electronics Division, Eden Prairie, MN, 1979.

[115] S. Doniach and M. Šunjić, *J. Phys. C*, **3**, 285 (1970).

[116] P.A. Redhead, *Vacuum*, **12**, 203 (1962).

[117] R.P.H. Gasser, "An Introduction to Chemisorption and Catalysis by Metals," Oxford University Press, 1985.

[118] D.G. Castner, B.A. Sexton, and G.A. Somorjai, *Surf. Sci.*, **71**, 519 (1978).

[119] P.A. Thiel, E.D. Williams, J.T. Yates, Jr., and W.H. Weinberg, *Surf. Sci.*, **84**, 54 (1974).

[120] R.J. Baird, R.C. Ku, and P. Wynblatt, *Surf. Sci.*, **97**, 346 (1980).

[121] P.R. Watson and G.A. Somorjai, *J. Phys. Chem.*, **86**, 3993 (1982).

[122] M.A. Logan and G.A. Somorjai, *J. Catal.*, **95**, 317 (1985).

[123] D.J. Dwyer, K. Yoshida, and G.A. Somorjai, "Adv. in Chem. Series," no. 178 (E.L. Kugler and F.W. Steffgen, Eds.), p. 65 (1979).

[124] G.C. Bond, G. Webb, P.B. Wells, and J.M. Winterbottom, *Trans. Faraday Soc.*, **62**, 443 (1966).

[125] F. Pinna, M. Gonizzi, G. Strukul, G. Cocco, and S. Enzo, *J. Catal.*, **82**, 171 (1983).

[126] U. Bardi and P.N. Ross, *J. Vac. Sci. Technol. A*, **2**(4), 1461 (1984).

[127] G.D. Davis, M. Natan, and K.A. Anderson, *Appl. Surf. Sci.*, **15**, 321 (1983).

[128] G.B. Raupp and J.A. Dumesic, *J. Phys. Chem.*, **89**, 5240 (1985).

[129] C.M. Greenlief, J.M. White, C.S. Ko, and R.J. Gorte, *J. Phys. Chem.*, **89**, 5025 (1985).

[130] C.R. Brundle and A.F. Carley, *Chem. Phys. Lett.*, **31**(3), 423 (1975).

[131] S.L.T. Andersson, *J. Chem. Soc.*, **75**, 1356 (1979).

[132] K. Wandelt, *Surf. Sci. Reports*, **2**, 1 (1982).

[133] J.H. Sinfelt, *Catal. Rev.*, **3**, 175 (1969).

[134] M. Salmeron, S. Ferrer, M. Jazzar, and G.A. Somorjai, *Phys. Rev. B*, **28**, 1158 (1983).

[135] C. Ocal, E. Martinez, and S. Ferrer, *Surf. Sci.*, **136**, 571 (1984).

[136] F. Falo, I. Cano, and M. Salmeron, *Surf. Sci.*, **143**, 303 (1984).

[137] B.C. Gates, J.R. Katzer, and G.C.A. Schuit, "Chemistry of Catalytic Processes," McGraw-Hill Book Company, 1979.

[138] Y.-W. Chung, W.J. Lo, and G.A. Somorjai, *Surf. Sci.*, **64**, 588 (1977).

[139] J.E. Huheey, "Inorganic Chemistry, Principles of Structure and Reactivity," 2nd Ed., Harper & Row, 1978.

[140] J.S. Rieck and A.T. Bell, *J. Catal.*, 1986, in press.

[141] N.K. Pande, Ph.D. Thesis, University of California, Berkeley, CA, 1985.

[142] M.A. Vannice, *J. Catal.*, 37, 449 (1975).

[143] T. Iizuka, Y. Tanaka, and K. Tanabe, *J. Catal.*, 76, 1 (1982).

[144] J.R. Budge, B.F. Løucke, B.G. Gates, and J. Toran, *J. Catal.*, 91, 272 (1985).

[145] F. Solymosi, I. Tombácz, and J. Koszta, *J. Catal.*, 95, 578 (1985).

[146] S.C. Chuang, J.G. Goodwin, Jr., and I. Wender, *J. Catal.*, 95, 435 (1985).

[147] J.B.F. Anderson, J.D. Bracey, R. Burch, A.R. Flambard, in "Proceedings, 8th International Congress on Catalysis," Vol. V, p. 111. Berlin, 1984.

[148] M.A. Vannice and C. Sudhakar, *J. Phys. Chem.*, 88, 2429 (1984).

[149] C. Sudhakar and M.A. Vannice, *J. Catal.*, 95, 227 (1985).

[150] W.M.H. Sachtler, in "Proceedings, 8th International Congress on Catalysis," Vol. V, p. 151. Berlin, 1984.

[151] W.M.H. Sachtler, D.F. Shriver, W.B. Hollenberg, and A.F. Long, *J. Catal.*, 92, 429 (1985).

[152] J.S. Rieck and A.T. Bell, *J. Catal.*, 96, 88 (1985).

[153] R.A. Dictor and A.T. Bell, *Appl. Catal.*, 20, 145 (1986).

[154] C.S. Kellner and A.T. Bell, *J. Catal.*, 70, 418 (1981).

[155] M. Boudart and G. Djéga-Mariadassou, "Kinetics of Heterogeneous Catalytic Reactions," Princeton University Press, 1984.

[156] J.L. Gland, *Surf. Sci.*, 93, 487 (1980).

Appendix A

FURTHER ANALYSIS OF OXIDE OVERLAYERS

A.1 ALTERNATIVE MEANS FOR DETERMINING OVERLAYER COVERAGE

An alternative method for the determination of oxide overlayer coverage has been employed in some studies [64,65]. The method involves comparing the AES O/Rh ratio for TiO_x on Rh with the ratio measured for O_2 chemisorbed (at saturation) on Rh. At 90 K, saturation coverage of O_2 on Rh resulted in an AES O/Rh ratio of 0.07 [65].

The difficulty in this method lies in applying the O/Rh value to the TiO_x overlayer. First of all, the actual coverage corresponding to saturation coverage of O_2 is uncertain. Saturation coverage is likely between 0.25 and 0.75 ML and may be a 2 x 2 overlayer (as with Pt [156]). However, the O/Rh ratio is of little value without a precise measure of the coverage.

If it is assumed that saturation coverage does correspond to 0.25 ML oxygen (a 2 x 2 overlayer), then the next step is to determine a basis for comparison with the AES O/Rh ratio of the TiO_x overlayer. The stoichiometry of the oxide overlayer is now important. Gorte *et al.* [65] observed an oxide overlayer of stoichiometry TiO. Based on this information, an AES O/Rh ratio of 0.19 was interpreted as "monolayer" coverage with a corresponding

33% attenuation in the Rh signal.

In the present work, monolayer coveage was determined from the linear break in an AES intensity-vs.-evaporation time plot. The O/Rh ratio corresponding to monolayer coverage was 0.96 for an oxide stoichiometry near TiO_2. If the oxide overlayer is "allowed" to have a three-dimensional structure, i.e., the monolayer is actually a bi-layer, then the monolayer equivalent of oxygen atoms on the surface is 2/3 x 2 ML = 1.33 ML, compared with 0.25 ML for the 2 x 2 oxygen overlayer. Taking into account the attenuation of the Rh signal (66%) yields a predicted AES O/Rh ratio of 0.85 at monolayer coverage. This represents a difference of only 13%. These calculations are illustrated below. Clearly, the method of coverage determination involving comparison of O/Rh ratios is consistent with both Gorte's calibration and the one presented here, although CO chemisorption data indicate a factor of three or four difference between these two calibrations.

For monolayer coverage for AlO_x on Rh (as determined from Fig. 5.5), an AES O/Rh ratio of about 0.43 was observed. The predicted value for a two-dimensional bi-layer is 0.63. However, since the degree of attenuation is smaller (α larger) for AlO_x/Rh compared with TiO_x/Rh at monolayer coverage, the assumption of a full bi-layer may not be valid. If the second layer is only half occupied, with O atoms on top, an AES O/Rh ratio of 0.50 might be expected.

The problem in this method lies in assumptions made of the oxide overlayer structure. One cannot compare O/Rh ratios in a meaningful manner unless the orientation of oxygen in the overlayer is known. For example, for a TiO overlayer, if the oxide exists as a lattice of Ti atoms on the surface with oxygen atoms sitting on top, twice as many oxygen atoms will exist on the surface compared with the case of O and Ti in the same plane. This method, therefore, is only as good as the available knowledge regarding the structure of the oxide overlayer. In the absence of this knowledge, many results are possible, depending on the structure assumed.

TiO_x/Rh Calculations:

I_{Rh}

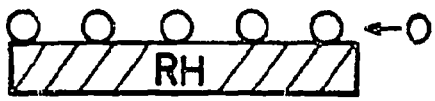

0.25 ML O on Rh $\quad \frac{I_O}{I_{Rh}} = 0.07$

1 ML ($\equiv$ 2 ML—bi-layer) $\quad \frac{I_O}{I_{Rh}} = ?$

#O atoms = (2 ML atoms) x $\frac{2}{5} = \frac{4}{5}$ ML

$\alpha = 0.34$: for a 1 atom thick monolayer, $\alpha' = \sqrt{0.34} = 0.58$

O on Rh: $\frac{I_O}{I_{Rh}} = 0.07 = \frac{y}{\underbrace{1-\frac{1-\sqrt{0.34}}{}}_{\text{0.25 ML attenuation of Rh}}} = 1.116\ y$

$\Rightarrow y = 0.0627$

TiO_2 on Rh: $\frac{I_O}{I_{Rh}} = \left(\frac{\frac{2}{5}\times 2ML}{0.25ML}\right) \frac{y}{1-0.66} \frac{\overbrace{1+\frac{1}{3}(0.66)}^{\text{attenuation of 1st layer O signal by 2nd layer O}}}{\frac{4}{5}} = 0.88$

Observed: $\frac{I_O}{I_{Rh}} = 0.96$

AlO_x/Rh Calculations:

I_{Rh}

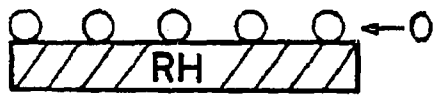

0.25 ML O on Rh $\qquad \frac{I_O}{I_{Rh}} = 0.07$

1 ML ($\equiv$ 2 ML—bi-layer) $\qquad \frac{I_O}{I_{Rh}} = ?$

#O atoms = (2 ML atoms) x $\frac{3}{5}$ = 1.1 ML

$\alpha = 0.45$: for a 1 atom thick monolayer, $\alpha' = \sqrt{0.45} = 0.67$

O on Rh: $\frac{I_O}{I_{Rh}} = 0.07 = \frac{y}{1-\underbrace{1-0.67}_{0.25\ ML\ attenuation\ of\ Rh}} = 1.090\ y$

$\Rightarrow y = 0.0642$

attenuation of 1st layer O signal by 2nd layer O

Al_2O_3 on Rh: $\frac{I_O}{I_{Rh}} = \left(\frac{\frac{3}{5}x2ML}{0.25ML}\right) \frac{y}{1-0.66} \overbrace{\frac{1+\frac{1}{3}(0.33)}{1.1}} = 0.66$

#O atoms = ("1.5 ML" atoms) x $\frac{3}{5}$ = 1.1 ML

$\alpha = 0.45$: for a "1.5 atom" thick monolayer, $\alpha' = \alpha^{\frac{1}{1.5}} = 0.45^{\frac{1}{1.5}} = 0.59$

O on Rh: $\frac{I_O}{I_{Rh}} = 0.07 = \frac{y}{\underbrace{1-\frac{1-0.59}{4}}_{\text{0.25 ML attenuation of Rh}}} = 1.090\ y$

$\Rightarrow y = 0.0628$

Al_2O_3 on Rh: $\frac{I_O}{I_{Rh}} = \left(\frac{\frac{3}{5}\times 1.5ML}{0.26ML}\right)\frac{y}{1-0.55} = 0.50$

Observed: $\frac{I_O}{I_{Rh}} = 0.43$

A.2 THE EFFECT OF THREE-DIMENSIONAL OVERLAYER GROWTH ON COVERAGE DETERMINATION

An analysis of the impact of three-dimensional overlayer growth on the measured AES substrate signal is presented here. Calculations were performed by assuming an overlayer geometry at a given coverage and calculating the attenuation of the substrate (Rh (302 eV)) signal. A value of α (the coverage) of 0.55 was taken. As seen from Table 2-1, this value is in the range observed for 280–360 eV electrons for overlayers of one atomic distance thickness. Since an attenuation corresponding to $\alpha = 0.34$ was observed for TiO_x/Rh, this analysis represents a worst-case scenario to test the validity of the coverage determination in Fig. 5.13.

Six overlayer geometries were employed, each comprised of stacked layers in which the angle formed between successive layers and the surface plane is specified. The overlayer geometries corresponding to angles of 0°, 18.4°, 32°,45°, 50° , and 78.7° are depicted in Fig. A.1 for a monolayer equivalent of 0.78 ML. The effect from only one island, of rectangular cross-section, on a section of substrate of arbitrary length was considered.

Fig. A.2 shows the resulting AES intensity-vs.-evaporation time plot for the various overlayer geometries. The AES intensities were normalized with respect to the bare substrate signal and the evaporation times normalized to give a 66% attenuation at the same time for all growth angles. This was done to compare with the analogous plot for TiO_x growth in Fig. 5.13(b). By comparison of the regions of initial decline in both plots, it is not possible to rule out the existence of three-dimensional growth of TiO_x for angles under, say, 45°. However, since a break does not occur at a substrate attenuation of 0.34 (remember $\alpha = 0.55$), the curves fall well below the trend for layer-by-layer growth displayed in Fig. 5.13(b). Consequently, the growth of titania on rhodium cannot be adequately described by three-dimensional growth.

The expected CO TPD area-versus-coverage plot for three-dimensional overlayer growth,

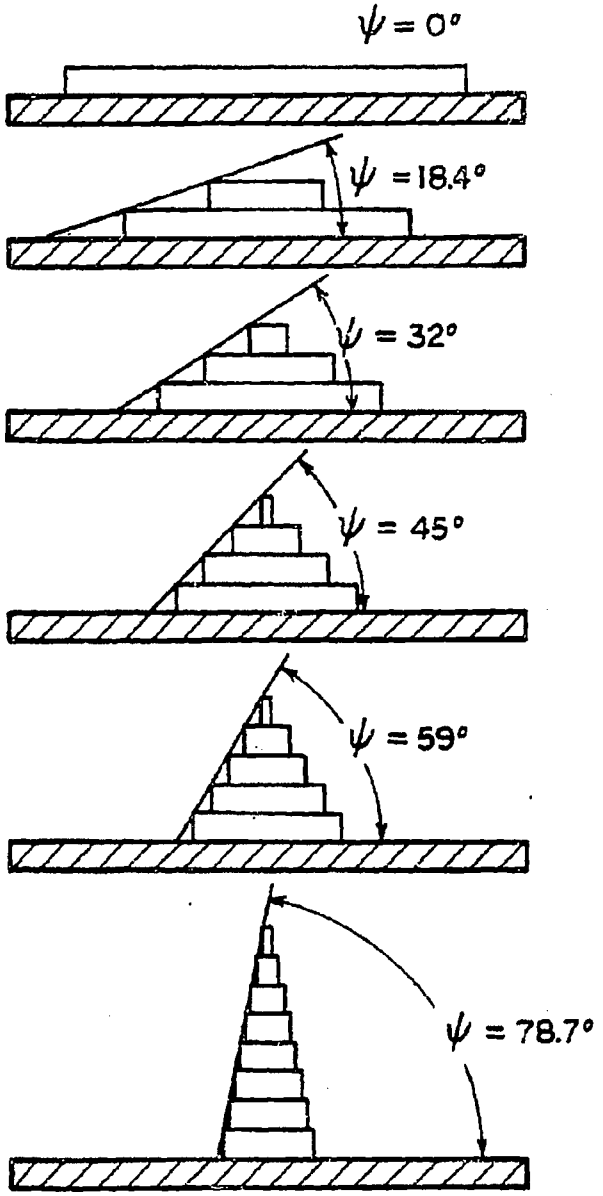

Figure A.1: Model geometries of overlayer growth. The extent of three-dimensional growth is characterized by the angle ψ between the surface and the incline of an overlayer "island".

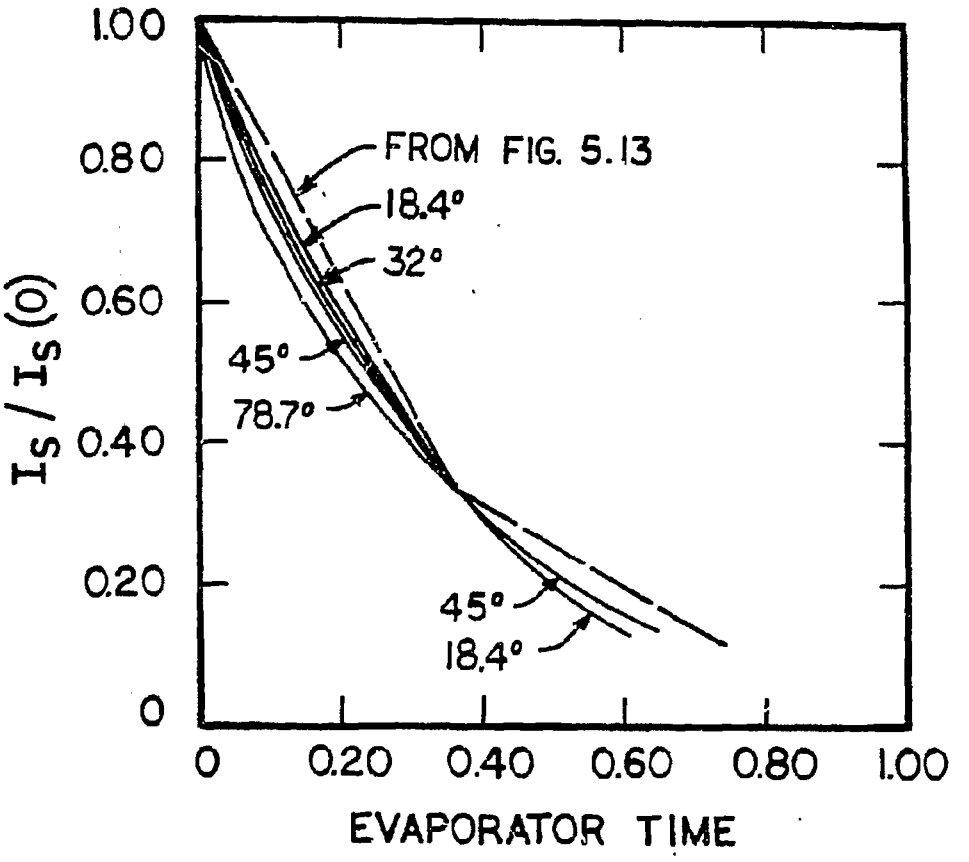

Figure A.2: A plot of the raw AES substrate intensity as a function of evaporation time. The curvature arising from three-dimensional growth is clearly visible for angles above 32°. The dosing times for an attenuation of 0.34 were set equivalent for comparison with Fig. 5-13(b).

assuming CO chemisorbs *at all exposed Rh sites*, appears in Fig. A.3. When three-dimensional growth occurs, the "apparent" coverage (measured by AES) does not accurately reflect the actual amount of surface Rh covered. As the "apparent" coverage increases, there is a nonlinear decrease in the CO chemisorption capacity. However, the amount of CO chemisorbed is always greater than that expected from the coverage. If coverage is determined from an attenuation of 66% at monolayer coverage, the CO TPD area-vs.-coverage plot of Fig. A.4 results. Three-dimensional growth can account for the behavior in Fig.

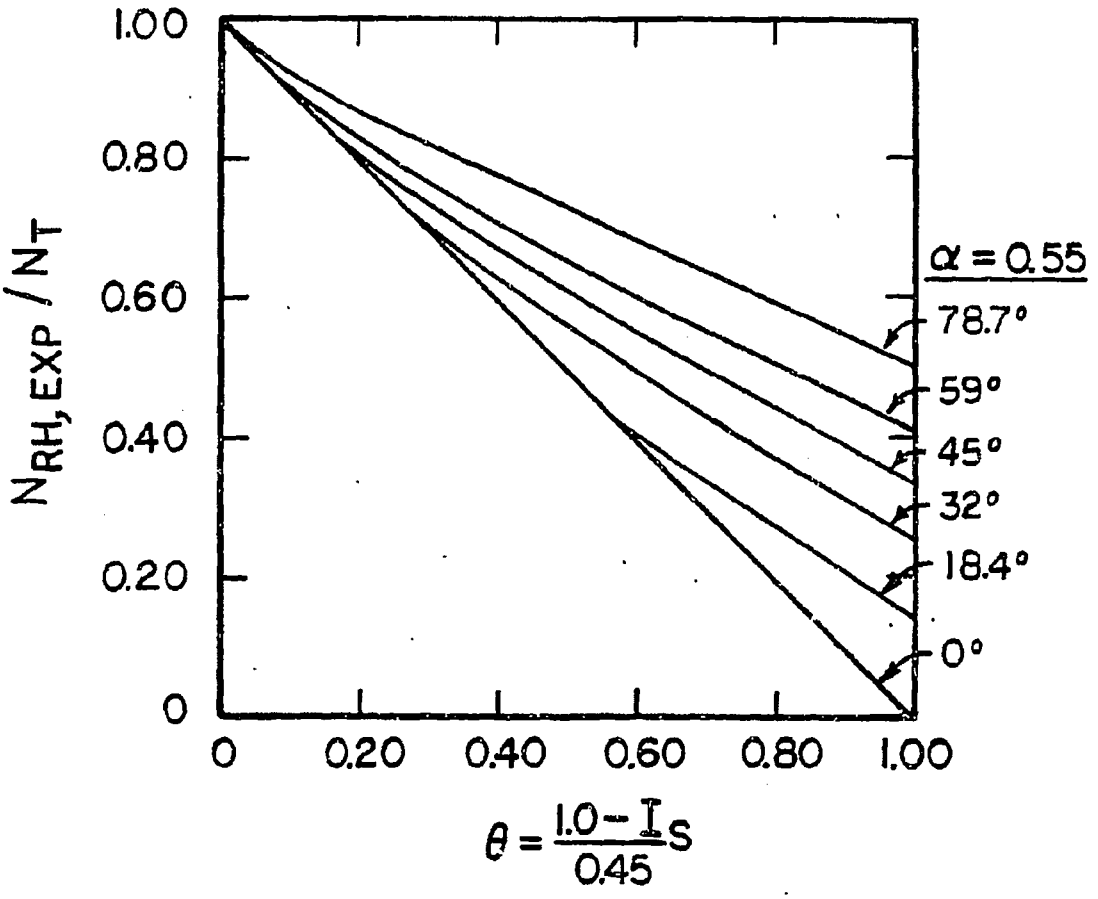

Figure A.3: The expected CO TPD peak area-vs.-coverage plots with three-dimensional overlayer growth and assuming CO chemisorbs at all exposed Rh atoms. $\alpha = 0.55$.

5.30 only if $\alpha = 0.77$ for monolayer coverage—an improbable value in light of the other overlayer studies in Table 2.1.

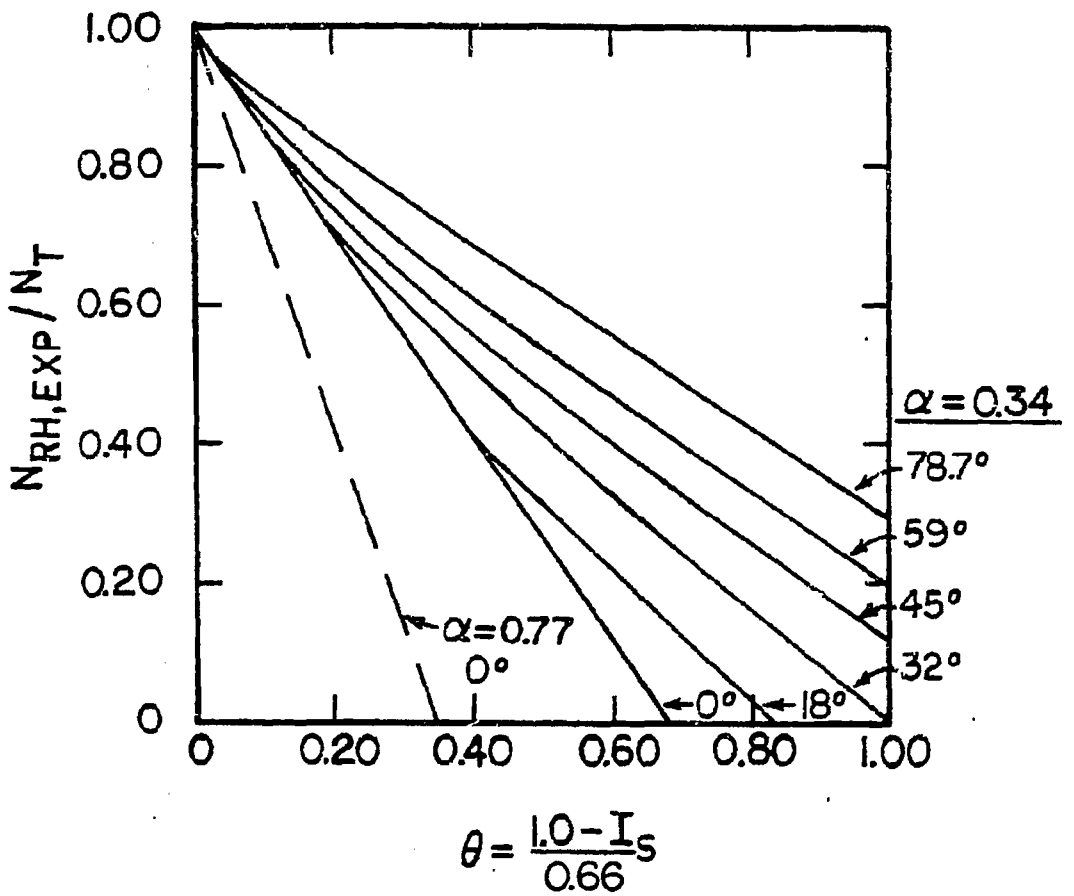

Figure A.4: The expected CO TPD peak area-vs.-coverage plots with three-dimensional overlayer growth and assuming CO chemsiorbs at all exposed Rh atoms. α taken as 0.34 with monolayer coverage actually at $\alpha = 0.55$—as a "worst case" evaluation of Fig. 5-30.

Appendix B

COMPUTER PROGRAMS

B.1 XPS DATA ACQUISITION AND ANALYSIS PROGRAM

The following program (written by Dr. Bruce Beard) was modified tc allow fitting of XPS spectra with peaks of Doniach-Šunjić lineshape (see Chapter 2). This program has a total of six function: (1) data acquisition, (2) analysis of stored data (Gaussian fit), (3) analysis of stored data (Doniach-Šunjić fit), (4) printing out raw data, (5) checking the contents of a data file, and (6) forming a data file of raw/analyzed data for future transferral to a mainframe computer. This program calculates a quantity, "deviation from the fit," by a sum of the squares of the difference between fitted and raw curves. However, there appears to be a "bug" in this part of the routine.

If any changes are to be made to this program, please adjust the timing loop (statement 4510) accordingly to match the IBM PC data acquisition timing with that of the Tracor multi-channel analyzer. Otherwise, an incomplete spectrum will be transferred to the IBM PC.

```
10 ' program electron spectroscopy
20 DIM X(520), Y(520), F(8,520), P(6,4), LOW(6), AREA(6), B(300), HF(6)
25 DIM A1(6),GAMMA(6),XB(3),YB(3),XE(256)
30 DEF SEG=&HB100     'SET ADDRESS LOCATION OF THE LAV MASTER BOARD.
40 POKE 3,4           'SET OUTPUT OF D/A THAT CONTROLS MCA DATA DUMP TO ~5 V.
50 POKE 2,0
55 NP=512
60 CMIN=0
70 SURSCN=0
75 PI=3.14159
80 'This is the main routine from which the remainder
90 'of the program is routed. Functions of this program include
100 'data collection, display, and a variety of routines
110 'necessary for the fittng analysis of XPS spectra.
120 'N represents the # of peaks to be fitted to the spectrum.
122 'This program was written by Dr.Bruce C. Beard in 1984. Modifications
123 'have been made to include peak subtraction, survey scan plotting,
124 'and more stream-lined data entry for fitting.
125 'This program was modified in Aug. 1986 by Marc Levin to allow for
126 'Doniach-Sunjic fitting of XPS spectra.  This modification includes
127 'subroutines for computing the Gamma function and a parabolic baseline
128 'from three points.  Changes were also made in the display routine to
129 'make it more efficient.
130 CLS
140 SCREEN 0
150 LOCATE 5,27
160 PRINT "SIX ROUTES ARE AVAILABLE"
170 LOCATE  6,23:PRINT "1.  Data Acquisition, XPS or AES"
180 LOCATE  7,23:PRINT "2.  Analysis of Stored Data--Gaussian Fit"
190 LOCATE  8,23:PRINT "3.  Analysis of Stored Data--Doniach-Sunjic Fit"
200 LOCATE  9,23:PRINT "4.  Hard Copy of Raw Data"
210 LOCATE 10,23:PRINT "5.  Check Contents of a Data File"
215 LOCATE 11,23:PRINT "6.  Disk Copy of Smoothed Data"
220 LOCATE 12,23:PRINT "9.  To Stop Program"
250 LOCATE 14,18
260 PRINT "Enter number for the desired option"
270 LOCATE 16,30
280 INPUT "OPTION ? . ",IDEX
290 SURSCN=0
300 FLG=0
310 IF IDEX=1 THEN GOSUB 3540
320 IF IDEX=2 THEN GOSUB 420
330 IF IDEX=3 THEN GOSUB 7420
340 IF IDEX=4 THEN GOSUB 5100
350 IF IDEX=5 THEN GOSUB 5250
355 IF IDEX=6 THEN GOSUB 7000
360 IF IDEX=9 THEN STOP
380 INPUT "Any further options (Y OR N)?",YN$
385 IF YN$<>"N" AND YN$<>"Y" THEN 380
390 IF YN$="Y" THEN 130
400 STOP
410 '
420 'Subroutine data analysis
430 'This routine fits data to as many as six gaussian components,
440 'satellite peak removal, baseline addition, and smoothing
450 ' are all available from this conrtolling subroutine.
460 '
465 LOCATE 2,23:PRINT "ANALYSIS OF STORED DATA--GAUSSIAN FIT"
470 GOSUB 3920
480 GOSUB 1770
```

```
490 GOSUB 2390
491 '
492 IF SURSCN=0 GOTO 500
493 INPUT "Hard copy (Y OR N)?   ",YN$
494 IF YN$<>"N" AND YN$<>"Y" THEN 493
495 IF YN$="N" THEN 130
496 GOSUB 2390
497 GOSUB 4620
498 GOTO 130
499 '
500 INPUT "Shall any smoothing of the data be performed (Y OR N)?  ",YN$
505 IF YN$<>"N" AND YN$<>"Y" THEN 500
510 IF YN$="Y" THEN GOSUB 1910
520 INPUT "Shall satellite removal be performed (Y OR N)?  ",YN$
525 IF YN$<>"N" AND YN$<>"Y" THEN 520
530 IF YN$="Y" THEN GOSUB 1580
540 INPUT "How many components to this spectrum?  ",N
550 IF N>6 GOTO 570 ELSE GOTO 590
560 BEEP
570 PRINT N,"IS TOO LARGE A VALUE FOR THE NUMBER OF COMPONENTS, TRY AGAIN"
580 GOTO 540
590 Z=N+2
600 PRINT"Enter the parameters for each component, Amp, eV, FWHM,"
610 FOR L=1 TO N
620 PRINT "Parameters for component #",L
630 FOR J=1 TO 3
640 PRINT "Enter p("L,J")"
650 INPUT P(L,J)
660 NEXT J
670 NEXT L
680 INPUT "PARAMETERS ENTERED CORRECTLY (Y OR N)?   ",YN$
685 IF YN$<>"N" AND YN$<>"Y" THEN 680
690 IF YN$="N" THEN GOTO 600
700 '
710 'CALCULATES THE GAUSSIAN LINE SHAPE FOR EACH OF THE COMPONENTS AND'
720 'THE SUMMATION; ALSO THE BACKGROUND INTENSITY DROP AND THE BASE-
730 'LINE CONTRIBUTION FROM EACH COMPONENT.'
740 '
750 INPUT "Enter beginning and ending background reference channels ",FRT1,BCK1
760 FRT=0: BCK=0: DEL=0
770 FOR K=1 TO 10
780 FRT=FRT+Y(FRT1+K)
790 BCK=BCK+Y(BCK1+K)
800 NEXT K
810 DEL=FRT/10-BCK/10
820 '
830 'TOTAL PEAK HEIGHTS
840 '
850 HGT=0
860 FOR K=1 TO N
870 HGT=HGT+P(K,1)
880 NEXT K
890 '
900 'CALCULATE THE BASELINE AND PEAKS
910 '
920 FOR K=1 TO N
930 HF(K)=P(K,1)/HGT
940 FOR J%=1 TO 256
950 DX=(X(J%)-P(K,2))/P(K,3)
960 F(K+1,J%)=P(K,1)*(1/EXP(DX*DX))
```

```
970 F(1,J%)=HF(K)*DEL/(1+EXP(-DX))
980 B(J%)=B(J%)+F(1,J%)
990 F(K+1,J%)=F(K+1,J%)+F(1,J%)
1000 F(Z,J%)=F(Z,J%)+F(K+1,J%)
1010 NEXT J%
1020 NEXT K
1030 '
1040 IF FLG=7 GOTO 1440
1050 IF FLG=5 THEN GOSUB 5880
1060 '
1070 'Section to allow for the correction of the parameters
1080 '
1090 GOSUB 2810
1100 LOCATE 24,1
1110 INPUT "Changes in the fit (Y OR N)?  ",YN$
1115 IF YN$<>"N" AND YN$<>"Y" THEN 1110
1120 IF YN$="Y" THEN GOTO 1130 ELSE 1270
1130 INPUT "Shall the number of components be changed (Y OR N)?  ",YN$
1135 IF YN$<>"N" AND YN$<>"Y" THEN 1130
1140 IF YN$="Y" GOTO 540
1150 INPUT "Change background?, (answer 0), or component # ?", L
1160 IF L=0 THEN GOTO 750
1170 IF L>N THEN BEEP ELSE GOTO 1200
1180 PRINT "Enter a number between 1 and  ",N
1190 GOTO 1150
1200 PRINT "Parameters for component # ",L
1210 FOR J=1 TO 3
1220 PRINT "Old P("L,J") value is:" ,P(L,J)
1230 INPUT "Enter new Value  ", CHECK
1240 IF CHECK=0 THEN GOTO 1250 ELSE P(L,J)=CHECK
1250 NEXT J
1260 GOTO 850
1270 '
1280 CLS
1290 LOCATE 5,25
1300 PRINT "THREE OPTIONS ARE AVAILABLE"
1310 LOCATE 8,25
1320 PRINT "1. PLOT FITTED SPECTRUM"
1330 LOCATE 10,25
1340 PRINT "2. SUBTRACT FITTED COMPONENTS"
1345 LOCATE 12,25: PRINT "3. EXIT ANALYSIS SECTION
1350 LOCATE 13,25
1360 BEEP
1370 INPUT " ENTER OPTION  ",IDEX
1380 IF IDEX=2 GOTO 5880
1385 IF IDEX=3 THEN RETURN
1387 IF IDEX<>1 GOTO 1370
1390 FLG=7
1400 GOTO 850
1410 '
1420 ' Calcuate area of each component.
1430 '
1440 FOR I=1 TO N
1450 AREA(I)=P(I,1)*P(I,3)*2.5066
1460 NEXT I
1470 '
1480 'Final display of fit with all the parameters, specimen description
1490 ' the area of each peak, and standard deviation of the fit.
1500 '
1510 LOCATE 17,15
```

```
1520 INPUT "** TURN ON THE PRINTER * STRIKE CARRIAGE RETURN **",YN$
1530 GOSUB 2810
1540 GOSUB 4650
1550 INPUT "PERFORM SUBTRACTION (Y OR N)? ",YN$
1555 IF YN$<>"N" AND YN$<>"Y" THEN 1550
1560 IF YN$="Y" THEN FLG=5:GOTO 850
1570 RETURN
1580 ' Subroutine Satpeak
1590 ' This routine removes the naturally occuring satellite peaks from the
1600 ' Mg Ka X-ray emission line used for XPS analysis.
1610 AU2=.085
1620 AU3=.045
1630 XINC=(X(1)-X(512))/256
1640 IAU2%=(8.45/XINC)
1650 IAU3%=(10.15/XINC)
1660 FOR J%=1 TO 256
1670 ID2=J%-IAU2%
1680 ID3=J%-IAU3%
1690 IF ID2<1 THEN ID2=1
1700 IF ID3<1 THEN ID3=1
1710 A3=Y(ID2)*AU2+Y(ID3)*AU3
1720 Y(J%)=Y(J%)-A3
1730 NEXT J%
1740 GOSUB 2390
1750 RETURN
1760 '
1770 'Subroutine loadx
1780 'This routine generates the x-array based on the number of channels
1790 'and the eV range.
1800 '
1810 XINC=(X(1)-X(512))/256
1820 IF X(1)>X(512) THEN GOTO 1870
1830 FOR I%=2 TO 256
1840 X(I%)=X(I%-1)+XINC
1850 NEXT I%
1860 GOTO 1900
1870 FOR I%=2 TO 256
1880 X(I%)=X(I%-1)-XINC
1890 NEXT I%
1900 RETURN
1905 '
1910 'Subroutine Smooth
1920 'This routine is a modified six point smoothing routine
1930 'where the operator is able to choose the degree of smoothing
1940 'by the use of a discriminator, the larger the disc value
1950 ' the smaller the change caused by the smoothing routine.
1960 INPUT "Enter the discriminator value   ",DISC
1970 GOSUB 2090
1980 SPRED=DISC*SQR(CMAX)
1990 FOR J%=4 TO 253
2000 AV=(Y(J%-3)+Y(J%-2)+Y(J%-1)+Y(J%+1)+Y(J%+2)+Y(J%+3))/6
2010 DIF=Y(J%)-AV
2020 ADIF=ABS(DIF)
2030 IF ADIF<SPRED THEN GOTO 2040 ELSE Y(J%)=AV
2040 NEXT J%
2050 GOSUB 2390
2060 INPUT "MORE SMOOTHING (Y OR N)? ",YN$
2065 IF YN$<>"N" AND YN$<>"Y" THEN 2060
2070 IF YN$="Y" THEN 1960
2080 RETURN
```

```
2085 '
2090 'Subroutine Maxmin
2100 'This routine determines the maximum and minimum values in the
2110 'data array
2120 CMAX=-50000!
2130 CMIN=90000!
2140 FOR J%=1 TO NP
2150 IF Y(J%)<CMIN THEN CMIN=Y(J%)
2160 IF Y(J%)>CMAX THEN CMAX=Y(J%)
2170 NEXT J%
2180 RETURN
2185 '
2190 'Subroutne normalize
2200 'this routine normalizes the data array to betwwen 0 and 1.
2210 CC=CMAX-CMIN
2220 FOR J%=1 TO NP
2230 Y(J%)=(Y(J%)-CMIN)/CC
2240 NEXT J%
2250 RETURN
2255 '
2260 'Subroutine SDFIT
2270 'This routne calculates the standard devaiton between the
2280 ' raw data and the fitted array, giving an indication of the
2290 ' goodness of the fitting paramters used.
2300 SUM=0
2310 FOR J%=1 TO 256
2320 F(Z,J%)=F(Z,J%)/CC
2330 SUM=SUM+(F(Z,J%)-Y(J%))^2
2340 F(Z,J%)=F(Z,J%)*CC
2350 NEXT J%
2360 SD=SQR(SUM/256)
2370 RETURN
2380 '
2390 'Subroutine Show
2400 ' This is a display routine which makes a simple plot of the data
2410 '
2420 SCREEN 2
2430 GOSUB 2090
2440 GOSUB 2190
2450 CLS
2460 LINE (99,15)-(611,15)
2470 LINE (611,15)-(611,175)
2480 LINE (611,175)-(99,175)
2490 LINE (99,175)-(99,15)
2500 '
2510 FOR I=1 TO 6
2520 LOCATE 7-I,6
2530 PRINT MID$ ("COUNTS",I,1)
2540 NEXT I
2550 '
2560 LOCATE 3,8
2570 PRINT CMAX
2580 LOCATE 22,8
2590 PRINT CMIN
2600 LOCATE 23,37
2602 IF X(1)<X(512) THEN GOTO 2614
2610 PRINT "BINDING ENERGY(eV)"
2612 GOTO 2620
2614 PRINT "KINETIC ENERGY(eV)"
2620 LOCATE 23,10
```

```
2630 PRINT X(1)
2640 LOCATE 23,74
2650 PRINT X(512)
2660 '
2670 IF SURSCN=1 THEN GOSUB 6230
2680 IF SURSCN=1 THEN GOTO 2790
2690 '
2700 I=0
2710 FOR J=1 TO NP
2720 COLMN=98+I
2730 I=I+(512/NP)
2740 Y(J)=Y(J)-1
2750 F(1,J)=(Y(J)*-160)+15
2755 'LPRINT J;COLMN;Y(J);F(1,J)
2760 PSET(COLMN,F(1,J))
2770 Y(J)=(Y(J)+1)*CC
2780 NEXT J
2790 RETURN
2800 '
2810 'Subroutine Shwal
2820 'Routine show-all plots the results of the data anaysis by displaying
2830 'the raw data, the fitted line, and each component in the fitted line.
2840 '
2850 '
2860 GOSUB 2090
2870 '
2880 CLS
2890 LINE (99,15)-(611,15)
2900 LINE (611,15)-(611,175)
2910 LINE (611,175)-(99,175)
2920 LINE (99,175)-(99,15)
2990 '
3000 FOR I=1 TO 10
3010 LOCATE 6+I,3
3020 PRINT MID$ ("NORMALIZED",I,1)
3030 NEXT I
3040 '
3050 FOR I=1 TO 6
3060 LOCATE 8+I,6
3070 PRINT MID$ ("COUNTS",I,1)
3080 NEXT I
3090 '
3100 LOCATE 2,8
3110 PRINT "1"
3140 '
3150 'normalize raw and fitted array,normalize components, and inert to 0 to -1
3160 '
3170 CC=CMAX-CMIN
3180 FOR J=1 TO 256
3190 Y(J)=(Y(J)-CMIN)/CC
3200 '
3205 FOR K=1 TO N+2
3210 F(K,J)=F(K,J)/CC
3215 NEXT K
3220 '
3230 ' plot raw data as a point plot ,raw data for plot in f(1,j)
3240 '
3250 PSET (97+2*J,160-Y(J)*160+15)
3260 'Y(J)=Y(J)*CC+CMIN
3270 NEXT J
```

```
3280 '
3290 'plot fitted data and individual components as lines
3300 '
3330 FOR J=1 TO 256
3335 PSET (97+2*J,160-Y(J)*160+15)
3336 Y(J)=Y(J)*CC+CMIN
3340 FOR K=1 TO N+2
3350 LINE (97+2*J,160-F(K,J)*160+15)-(99+2*J,160-F(K,J-1)*160+15)
3360 F(K,J)=F(K,J)*CC
3370 NEXT K
3380 NEXT J
3390 '
3420 LOCATE 22,8
3430 PRINT "0"
3435 LOCATE 23,10
3440 PRINT X(1)
3450 LOCATE 23,37
3455 IF X(1)<X(512) THEN GOTO 3466
3460 PRINT "BINDING ENERGY(eV)"
3464 GOTO 3470
3466 PRINT "KINETIC ENERGY(eV)"
3470 LOCATE 23,74
3480 PRINT X(512)
3520 RETURN
3530 '
3540 'Subroutine Data Acquisiton
3550 'Controls the input of data into the computer assuring
3560 'all of the pertinent details are present.
3570 INPUT "Enter the energy values X(1),X(512)",X(1),X(512)
3580 'date of analysis obtained from system
3590 VS=DATE$
3600 INPUT "Enter specimen description.",SPMNS
3610 PRINT "Enter the analysis conditions, transition, RC, Resolution,"
3620 INPUT "Vmult, Excitation Energy.",CONS
3630 INPUT "How many scans ?",SCANS$
3640 IF X(1)>X(512) THEN GOSUB 4290 ELSE GOSUB 5380
3650 '
3660 BEEP
3670 '
3680 'data collection completed
3690 '
3700 NP=512
3705 GOSUB 2390
3710 INPUT "Shall this data be stored (Y OR N)?",YNS
3715 IF YNS<>"N" AND YNS<>"Y" THEN 3710
3720 IF YNS="N" THEN 3740
3722 GOSUB 3760
3725 INPUT"HARD COPY OF STORED DATA (Y OR N)?",YNS
3730 IF YNS<>"N" AND YNS<>"Y" THEN 3725
3732 IF YNS="N" THEN RETURN
3734 GOSUB 3970
3736 GOSUB 2390
3738 GOSUB 4650
3740 RETURN
3750 '
3760 'Subroutine Store, This routine accepts the collected data and analysis
3770 ' discription and places them on the data disk for future reference.
3780 '
3790 INPUT "Enter the name under which this data shall be filed",NAMS
3800 OPEN NAMS FOR OUTPUT AS #1
```

```
3810 PRINT #1, SPMN$
3820 PRINT #1, VS
3830 PRINT #1, SCANS$
3840 PRINT #1, CON$
3850 PRINT #1, X(1),X(512)
3860 FOR J=1 TO 512
3870 PRINT#1, Y(J)
3880 NEXT J
3890 CLOSE #1
3900 RETURN
3910 '
3920 'Subroutine Recall, This routine retreves the desired data file from
3930 'the data disk, loading all the information into the proper string
3940 'or array.
3950 LOCATE 16,13
3960 INPUT "What is the name of the desired data file?  ",NAM$
3970 OPEN NAM$ FOR INPUT AS #1
3980 INPUT #1, SPMN$
3990 INPUT #1, VS
4000 INPUT #1, SCANS$
4010 INPUT #1, CON$
4020 INPUT #1, X(1),X(512)
4030 FOR J%=1 TO 512
4040 INPUT #1, Y(J%)
4050 NEXT J%
4060 '
4070 BEDIF=X(1)-X(512)
4080 IF BEDIF<100 THEN GOTO 4140
4090 PRINT "Binding energy difference has been found to be > 100 eV"
4100 INPUT "Shall all 512 data points be displayed (Y OR N)? ",YN$
4105 IF YN$<>"N" AND YN$<>"Y" THEN 4100
4110 IF YN$="N" THEN 4140
4120 SURSCN=1
4130 GOTO 4200
4140 '
4150 ' Reduce the 512 data points to 256 for numeric evaluation.
4160 '
4170 FOR K%=1 TO 256
4180 Y(K%)=(Y(2*K%-1)+Y(2*K%))/2
4190 NEXT K%
4200 'y(1) and y(2) are noisy channels, thus they
4210 'are set to the average of three points which follow.
4220 Y(1)=(Y(3)+Y(4)+Y(5))/3
4230 Y(2)=(Y(4)+Y(5)+Y(6))/3
4240 IF SURSCN=1 THEN GOTO 4260
4250 NP=256
4260 CLOSE #1
4270 RETURN
4280 '
4290  'Subroutine XPSAQ
4300 'This is a data retreal reutine taking data from the Tracor MCA
4310 'into the PC, correcting for the number of channels used in the
4320 'A/D conversion and the vertical scale factor of the MCA.
4330 '
4420 PRINT "********SET OUPUT RATE OF MCA TO 40 MS/CHAN*******"
4430 INPUT "Enter the vertical scale factor from the MCA",VSF
4440 DEF SEG=&HB100
4450 POKE 5,0                        'SELECT A/D CHANNEL
4460 POKE 3,0
4470 POKE 2,200                     'SET D/A #1 TO 0 VOLTS START DATA OUT
```

```
4480 FOR J=1 TO 512
4490 POKE 6,1                          'START CONVERSION
4500 Y(J)=256*PEEK (6) + PEEK (5)
4510 FOR Z=1 TO 60:NEXT Z 'MCA OUTPUT SPEED 40 MS/CHAN--READJUSTED FOR ESCA1
4520 NEXT J
4530 BEEP
4540 POKE 3,4                          'RESET D/A TO 5 V
4550 POKE 2,0
4560 '
4570 FOR I%=1 TO 512
4580 Y(I%)=Y(I%)*VSF/2048          'OUTPUT OF MCA ONLY 0-5, DA SET FOR 0-10
4590 NEXT I%
4600 '
4610 RETURN
4620 'Screen dump routine for the IBM PC to an HP Think-Jet printer
4630 'This routine was written by David Dahlgren,
4640 '
4650 DIM IMASK%(10)
4660 IMASK%(0)=1:IMASK%(1)=2:IMASK%(2)=4:IMASK%(3)=8:IMASK%(4)=16:IMASK%(5)=32
4670 IMASK%(6)=64:IMASK%(7)=128
4680 DEF SEG=&HB800
4690 OFST%=&H2000
4700 LPRINT                'CLEAR PRINTER
4710 LPRINT CHR$(27)+CHR$(64)
4720 WIDTH "LPT1:",255    'QUENCH CARRIAGE RETURNS
4730 LPRINT CHR$(27)+CHR$(65)+CHR$(8);         '16 DOT LINE FEED
4740 FOR         ROW%=0 TO 49
4750 IROW%=ROW%*160
4760 LPRINT CHR$(27)+CHR$(75)+CHR$(128)+CHR$(2);      'RECEIVE 640 BYTES
4770   FOR COL%=0 TO 79
4780    ICOL%=IROW%+COL%
4790    CH%=0                          'START WITH BLANK
4800    FOR BIT%=7 TO 0 STEP  -1
4810      MASK%=IMASK%(BIT%)
4820      IF (PEEK(ICOL%+80+OFST%) AND MASK%)>0 THEN CH%=CH% OR 3
4830      IF (PEEK(ICOL%+80) AND MASK%)>0       THEN CH%=CH% OR 12
4840      IF (PEEK(ICOL%+OFST%) AND MASK%)>0    THEN CH%=CH% OR 48
4850      IF (PEEK(ICOL%) AND MASK%)>0          THEN CH%=CH% OR 192
4860      LPRINT CHR$(CH%);:CH%=0
4870    NEXT
4880   NEXT
4890   LPRINT
4900 NEXT
4910 LPRINT CHR$(27)+CHR$(50)
4920 LOCATE 24,1
4930 LPRINT "Data file name:",NAM$
4940 LPRINT "Specimen",SPMN$
4950 LPRINT "Analysis Date:",V$
4960 LPRINT "Analysis Conditions",CON$
4970 LPRINT "Number of Scans:",SCAN$$
4980 INPUT "Shall the fitting parameters & areas be printed (Y OR N)?",YN$
4985 IF YN$<>"N" AND YN$<>"Y" THEN 4980
4990 IF YN$="N" THEN 5070
5000 LPRINT
5010 LPRINT "PEAK #","COUNTS","POSITION (eV)","WIDTH (eV)","ASYMMETRY","AREA"
5020 FOR J=1 TO N
5030 LPRINT J,P(J,1),P(J,2),P(J,3),P(J,4),AREA(J)
5040 NEXT J
5045 LPRINT XB(1),YB(1),XB(2),YB(2),XB(3),YB(3)
5050 GOSUB 2260
```

```
5060 LPRINT "Deviation of the Fit",SD
5070 RETURN
5080 '
5090 '
5100 'Subroutine display files, Reads a data file from the disk, allows for
5110 'satellite removal and smoothing before the spectrum is sent to the
5120 'screen dump.
5130 GOSUB 3920
5140 GOSUB 2390
5150 INPUT "Shall satellite removal be performed (Y OR N)?",YN$
5155 IF YN$<>"N" AND YN$<>"Y" THEN 5150
5160 IF YN$="Y" THEN GOSUB 1580
5170 INPUT "Shall any smoothing be performed (Y OR N)?",YN$
5175 IF YN$<>"N" AND YN$<>"Y" THEN 5170
5180 IF YN$="Y" THEN GOSUB 1910
5190 INPUT "TURN ON PRINTER!!! STRIKE RETURN WHEN READY",YN$
5200 GOSUB 2390
5210 GOSUB 4650
5220 RETURN
5230 '
5240 '
5250 'Subroutine file check. Reads data files, lists specimen description
5260 'and analysis date.
5270 GOSUB 3920
5280 GOSUB 2390
5290 PRINT SPMN$
5300 PRINT "Analysis Date:",V$
5310 INPUT "Shall data analysis be performed (Y OR N)?",YN$
5315 IF YN$<>"N" AND YN$<>"Y" THEN 5310
5320 IF YN$="Y" THEN 490 ELSE GOTO 5340
5330 RETURN
5340 INPUT "Is a hard copy of the raw data desired (Y OR N)?",YN$
5345 IF YN$<>"N" AND YN$<>"Y" THEN 5340
5350 IF YN$="Y" THEN GOSUB 2390 ELSE 5370
5360 GOSUB 4620
5370 RETURN
5380 'SUBROUTINE AUGERAQ
5390 'Acquires Auger data, controls output of diriving voltage
5400 'converts analog data to digital values, sums and averages
5410 'signal over the desired number of scans.
5420 '
5430 DEF SEG=&HB100
5440 '
5450 POKE 5,1            'SET A/D CONVERSION CHANNEL
5460 H=0
5470 '
5480 INPUT "How many scans to be collected?",S
5490 '
5500 FOR I%=1 TO S
5510 '
5520 FOR J=8 TO 15
5530 POKE 1,J
5540 FOR K=0 TO 255 STEP 8        'VOLTAGE STEPS 0V TO 5V
5550 POKE 0,K
5560 FOR L=1 TO 20: NEXT L        'DEAD LOOP TO ALLOW VOLTAGES TO STABALIZE
5570 H=H+1
5580 POKE 6,1                     'START A/D CONVERSION
5590 Y(H)=Y(H) + (256 * PEEK(6) + PEEK(5))     'CONVERT AND SUM
5600 NEXT K
5610 NEXT J
```

```
5620 FOR J=0 TO 7                  'VOLTAGE STEPS 5V TO 10V
5630 FOR K=0 TO 255 STEP 8
5640 POKE 1,J
5650 POKE 0,K
5660 FOR L=1 TO 20: NEXT L          'DEAD LOOP TO ALLOW VOLTAGES TO STABALIZE
5670 H=H+1
5680 POKE 6,1                      'START A/D CONVERSION
5690 Y(H)=Y(H)+(256*PEEK(6)+PEEK(5))
5700 NEXT K
5710 NEXT J
5720 '
5730 POKE 1,8       'RESET D/A TO 0 VOLTS AHEAD OF TIME TO ALLOW THE OUTPUT
5740 POKE 0,0       'AT THE BEGINNING OF THE NEXT SCAN TO BE 0 VOLTS
5750 '
5760 H=0
5770 '
5780 NEXT I%
5790 '
5800 FOR J%=1 TO 512
5810 Y(J%)=Y(J%)/S           'AVERAGE RESULTS OVER THE NUMBER OF SCANS
5820 NEXT J%
5830 '
5840 BEEP
5850 RETURN
5860 '
5870 '
5880 '                        SUBROUTINE SUBTRACTION
5890 ' THIS ROUTINE TAKES THE FITTED COMPONENTS THAT ARE TO THE OPERATORS
5900 ' LIKING AND REMOVES THEM FROM THE RAW DATA FILE TO LEAVE A DIFFERENCE
5910 ' SPECTRUM. FURTHER FITTING AND OUTPUT OPTION FOLLOW THIS ROUTINE SUCH
5920 ' THAT COMPARISONS MAY BE MADE FROM BEFORE AND AFTER SUBTRACTIONS.
5930 '
5960 '
5970 FOR I%=1 TO 256
5980 Y(I%)=Y(I%)-F(Z,I%)
5990 NEXT I%
6000 '
6010 FLG=0
6020 '
6030 GOSUB 2390
6040 INPUT "ANY SMOOTHING (Y OR N)? ",YN$
6045 IF YN$<>"N" AND YN$<>"Y" THEN 6040
6050 IF YN$="Y" THEN GOSUB 1910
6060 LOCATE 24,1
6070 INPUT "HARD COPY (Y OR N)?",YN$
6075 IF YN$<>"N" AND YN$<>"Y" THEN 6070
6080 IF YN$="N" THEN GOTO 6110
6090 GOSUB 2390
6100 GOSUB 4650
6110 '
6120 FOR K=1 TO Z
6130 FOR I%=1 TO 256
6140 F(K,I%)=0
6150 NEXT I%
6160 NEXT K
6170 '
6180 FOR I%=1 TO 256
6190 B(I%)=0
6200 NEXT I%
6210 RETURN
```

```
6220 '
6230 'SUBROUTINE SURVEY SCAN PLOT
6240 'This is a short routine to just plot out the data array for a
6250 ' survey scan. All 512 data points are displayed.
6260 '
6270 FOR J=1 TO 512
6280 COLMN=98+J
6290 Y(J)=Y(J)-1
6300 F(1,J)=(Y(J)*-160)+15
6310 PSET(COLMN,F(1,J))
6320 Y(J)=(Y(J)+1)*CC
6330 NEXT J
6340 RETURN
7000 'Subroutine DiskStore.  This routine reads a datafile, allow removal
7002 'of satellites, allow for smoothing, and then saves the data on disk
7004 'for eventual transferral to the VAX system.
7010 GOSUB 3920
7015 GOSUB 2390
7020 INPUT "Is satellite removal to be performed (Y OR N)?", YN$
7025 IF YN$<>"N" AND YN$<>"Y" THEN 7020
7030 IF YN$="Y" THEN GOSUB 1580
7035 INPUT "Is any smoothing to be performed (Y OR N)?", YN$
7040 IF YN$<>"N" AND YN$<>"Y" THEN 7035
7045 IF YN$="Y" THEN GOSUB 1910
7050 INPUT "Enter the name under which this data is to be filed", NAM$
7055 OPEN NAM$ FOR OUTPUT AS #1
7060 PRINT #1, SPMN$
7065 PRINT #1, V$
7070 PRINT #1, SCANS$
7075 PRINT #1, CON$
7080 PRINT #1, X(1),X(512)
7085 FOR J=1 TO 256
7090 XE(J)=X(1) - (X(1)-X(512))/256*(J-1)
7092 PRINT #1, XE(J),Y(J)
7094 NEXT J
7098 INPUT "Is a disk copy of the deconvoluted spectra desired?", YN$
7099 IF YN$<>"N" AND YN$<>"Y" THEN 7098
7100 IF YN$="N" THEN 7394
7105 CLS
7110 LOCATE 2,19:PRINT "ANALYSIS OF STORED DATA (DONIACH-SUNJIC FIT)"
7120 GOSUB 1770
7125 GOSUB 2390
7130 '
7135 IF SURSCN=0 GOTO 7160
7140 GOSUB 2390
7145 GOSUB 4620
7150 GOTO 130
7155 '
7160 INPUT "How many components to this spectrum?  ",N
7165 IF N>6 GOTO 7175 ELSE GOTO 7195
7170 BEEP
7175 PRINT N,"IS TOO LARGE A VALUE FOR THE NUMBER OF COMPONENTS, TRY AGAIN"
7180 GOTO 7160
7195 Z=N+2
7200 PRINT"Enter the parameters for each component, Amp, eV, FWHM,ASYM"
7205 FOR L=1 TO N
7210 PRINT "Parameters for component #",L
7215 FOR J=1 TO 4
7220 PRINT "Enter p("L,J")"
7225 INPUT P(L,J)
```

```
7230 NEXT J
7235 NEXT L
7240 INPUT "PARAMETERS ENTERED CORRECTLY (Y OR N)?   ",YN$
7245 IF YN$<>"N" AND YN$<>"Y" THEN 7240
7250 IF YN$="N" THEN GOTO 7200
7255 '
7260 'THE SUMMATION; ALSO THE BACKGROUND INTENSITY DROP AND THE BASE-
7265 'LINE CONTRIBUTION FROM EACH COMPONENT.
7270 '
7275 GOSUB 2390
7280 INPUT "ENTER 1ST BASELINE REFERENCE POINT (CHANNEL,HEIGHT) ",XB(1),YB(1)
7285 INPUT "ENTER 2ND BASELINE REFERENCE POINT (CHANNEL,HEIGHT) ",XB(2),YB(2)
7290 INPUT "ENTER 3RD BASELINE REFERENCE POINT (CHANNEL,HEIGHT) ",XB(3),YB(3)
7295 GOSUB 9200
7300 '
7305 '
7310 '
7320 'CALCULATE THE BASELINE AND PEAKS
7325 FOR J%=1 TO 256
7330 F(Z,J%) = F(1,J%)
7335 NEXT J%
7340 '
7345 FOR K=1 TO N
7347 PRINT #1, "K = ", K
7350 A1(K)=1-P(K,4)
7355 GOSUB 9000
7360 FOR J%=1 TO 256
7362 M1=COS(PI*P(K,4)/2 + A1(K)*ATN((P(K,2)-X(J%))/P(K,3)))
7364 M2=((X(J%)-P(K,2))^2 + P(K,3)^2)^(A1(K)/2)
7366 F(K+1,J%)=P(K,1)*GAMMA(K)*M1/M2
7368 B(J%)=B(J%)+F(1,J%)
7370 F(Z,J%)=F(Z,J%)+F(K+1,J%)
7371 PRINT #1, X(J%),F(K+1,J%)
7372 NEXT J%
7374 NEXT K
7378 PRINT #1, "TOTAL"
7380 FOR J% =1 TO 256
7385 PRINT #1, X(J%),F(Z,J%)
7390 NEXT J%
7394 CLOSE #1
7395 RETURN
7410 '
7420 'Subroutine data analysis
7430 'This routine fits data to as many as six Doniach-Sunjic components,
7440 'satellite peak removal, baseline addition, and smoothing
7450 ' are all available from this conrtolling subroutine.
7460 '
7462 CLS
7465 LOCATE 2,19:PRINT "ANALYSIS OF STORED DATA (DONIACH-SUNJIC FIT)"
7470 GOSUB 3920
7480 GOSUB 1770
7490 GOSUB 2390
7491 '
7492 IF SURSCN=0 GOTO 7500
7493 INPUT "Hard copy (Y OR N)?   ",YN$
7494 IF YN$<>"N" AND YN$<>"Y" THEN 7493
7495 IF YN$="N" THEN 130
7496 GOSUB 2390
7497 GOSUB 4620
7498 GOTO 130
```

```
7499 '
7500 INPUT "Shall any smoothing of the data be performed (Y OR N)?  ",YN$
7505 IF YN$<>"N" AND YN$<>"Y" THEN 7500
7510 IF YN$="Y" THEN GOSUB 1910
7520 INPUT "Shall satellite removal be performed (Y OR N)?  ",YN$
7525 IF YN$<>"N" AND YN$<>"Y" THEN 7520
7530 IF YN$="Y" THEN GOSUB 1580
7540 INPUT "How many components to this spectrum?  ",N
7550 IF N>6 GOTO 7570 ELSE GOTO 7175
7560 BEEP
7570 PRINT N,"IS TOO LARGE A VALUE FOR THE NUMBER OF COMPONENTS, TRY AGAIN"
7580 GOTO 7540
7590 Z=N+2
7600 PRINT"Enter the parameters for each component, Amp, eV, FWHM,ASYM"
7610 FOR L=1 TO N
7620 PRINT "Parameters for component #",L
7630 FOR J=1 TO 4
7640 PRINT "Enter p("L,J")"
7650 INPUT P(L,J)
7660 NEXT J
7670 NEXT L
7680 INPUT "PARAMETERS ENTERED CORRECTLY (Y OR N)?   ",YN$
7685 IF YN$<>"N" AND YN$<>"Y" THEN 7680
7690 IF YN$="N" THEN GOTO 7600
7700 '
7720 'THE SUMMATION; ALSO THE BACKGROUND INTENSITY DROP AND THE BASE-
7730 'LINE CONTRIBUTION FROM EACH COMPONENT.
7735 '
7740 GOSUB 2390
7741 INPUT "ENTER 1ST BASELINE REFERENCE POINT (CHANNEL,HEIGHT) ",XB(1),YB(1)
7742 INPUT "ENTER 2ND BASELINE REFERENCE POINT (CHANNEL,HEIGHT) ",XB(2),YB(2)
7743 INPUT "ENTER 3RD BASELINE REFERENCE POINT (CHANNEL,HEIGHT) ",XB(3),YB(3)
7795 GOSUB 9200
7800 '
7820 '
7850 '
7900 'CALCULATE THE BASELINE AND PEAKS
7905 FOR J%=1 TO 256
7907 F(Z,J%) = F(1,J%)
7909 NEXT J%
7910 '
7920 FOR K=1 TO N
7925 A1(K)=1-P(K,4)
7930 GOSUB 9000
7940 FOR J%=1 TO 256
7955 M1=COS(PI*P(K,4)/2 + A1(K)*ATN((P(K,2)-X(J%))/P(K,3)))
7960 M2=((X(J%)-P(K,2))^2 + P(K,3)^2)^(A1(K)/2)
7970 F(K+1,J%)=P(K,1)*GAMMA(K)*M1/M2
7980 B(J%)=B(J%)+F(1,J%)
8000 F(Z,J%)=F(Z,J%)-F(K+1,J%)
8010 NEXT J%
8020 NEXT K
8030 '
8050 IF FLAG=5 THEN GOSUB 5880
8060 '
8065 'Section to allow for the correction of the parameters
8070 '
8075 GOSUB 2810
8080 LOCATE 24,1
8085 INPUT "Changes in the fit (Y OR N)?  ",YN$
```

```
8090 IF YN$<>"N" AND YN$<>"Y" THEN 8085
8095 IF YN$="N" THEN 8270
8100 INPUT "Shall the number of components be changed (Y OR N)?  ",YN$
8105 IF YN$<>"N" AND YN$<>"Y" THEN 8100
8110 IF YN$="Y" THEN 7540
8115 INPUT "Change background?, (answer 0), or component # ?", L
8120 IF L<>0 THEN 8145
8125 FOR J=1 TO 3
8127 PRINT"BASELINE REFERENCE POINT NUMBER";J;":",XB(J),YB(J)
8129 INPUT"ENTER NEW CHANNEL";XT
8130 IF XT=0 THEN 8133
8131 INPUT"ENTER NEW HEIGHT";YT
8132 XB(J)=XT:YB(J)=YT
8133 NEXT J
8134 FOR J=1 TO 256
8135 F(Z,J)=F(Z,J)-F(1,J)
8136 NEXT J
8137 GOSUB 9200
8139 GOTO 8200
8140 IF YN$="Y" THEN 7540
8145 IF L>N THEN BEEP ELSE GOTO 8160
8150 PRINT "Enter a number between 1 and  ",N
8155 GOTO 8115
8160 PRINT "Parameters for component # ",L
8165 FOR J=1 TO 4
8170 PRINT "Old P("L,J") value is:" ,P(L,J)
8175 INPUT "Enter new Value  ", CHECK
8180 IF CHECK=0 THEN GOTO 8185 ELSE P(L,J)=CHECK
8185 NEXT J
8200 FOR J=1 TO 256
8205 IF L=0 THEN 8245
8210 F(Z,J)=F(Z,J)-F(L+1,J)
8215 A1(L)=1-P(L,4):K=L
8220 GOSUB 9000
8225 M1=COS(PI*P(L,4)/2 + A1(L)*ATN((P(L,2)-X(J))/P(L,3)))
8230 M2=((X(J)-P(L,2))^2 + P(L,3)^2)^(A1(L)/2)
8235 F(L+1,J)=P(L,1)*GAMMA(L)*M1/M2
8240 B(J)=B(J)+F(1,J)
8245 F(Z,J)=F(Z,J)-F(L+1,J)
8250 NEXT J
8260 GOTO 8050
8270 '
8280 CLS
8290 LOCATE 5,25
8300 PRINT "FOUR OPTIONS ARE AVAILABLE"
8310 LOCATE 8,25
8320 PRINT "1. PLOT FITTED SPECTRUM"
8330 LOCATE 10,25
8340 PRINT "2. SUBTRACT FITTED COMPONENTS"
8345 LOCATE 12,25: PRINT "3. CONTINUE SPECTRUM FITTING
8350 LOCATE 14,25: PRINT "4. EXIT ANALYSIS SECTION
8360 LOCATE 16,25:BEEP
8370 INPUT " ENTER OPTION  ",IDEX
8380 IF IDEX=2 GOTO 5880
8385 IF IDEX=3 THEN GOTO 8065
8390 IF IDEX=4 THEN RETURN
8395 IF IDEX<>1 GOTO 8370
8400 '
8410 '
8420 ' Calcuate area of each component (Simpson's Rule Integration)
```

```
8425 '
8430 FOR K=1 TO N
8435 AREA(K)=0
8440 FOR J%=2 TO 256
8445 IF J%=2 OR J%=256 THEN AREA(K)=AREA(K)+F(K+1,J%):GOTO 8460
8450 IF J%/2*2=J% THEN AREA(K)=AREA(K)+2*F(K+1,J%):GOTO 8460
8455 AREA(K)=AREA(K)+4*F(K+1,J%)
8460 NEXT J%
8462 AREA(K)=AREA(K)/3
8465 NEXT K
8470 '
8480 'Final display of fit with all the parameters, specimen description
8490 ' the area of each peak, and standard deviation of the fit.
8500 '
8510 LOCATE 17,15
8520 INPUT "** TURN ON THE PRINTER * STRIKE CARRIAGE RETURN **",YN$
8530 GOSUB 2810
8540 GOSUB 4650
8550 INPUT "PERFORM SUBTRACTION (Y OR N)? ",YN$
8555 IF YN$<>"N" AND YN$<>"Y" THEN 8550
8560 IF YN$="Y" THEN FLG=5:GOTO 7850
8570 RETURN
9000 'SUBROUTINE GAMMA
9010 'THIS SUBROUTINE CALCULATES THE GAMMA FUNCTION FOR 1-ALPHA BY A
9020 'POLYNOMIAL APPROXIMATION (FROM HANDBOOK OF MATHEMATICAL FUNCTIONS
9030 'BY ABRAMOWITZ AND STEGUN).  THE VALUE OF X SHOULD BE BETWEEN 0 AND
9040 '1 FOR THIS APPROXIMATION, OR  0<ALPHA<1.
9050 GAMMA(K)=1 - .577192*A1(K) + .988206*A1(K)^2 - .89705^*A1(K)^3
9060 GAMMA(K)=GAMMA(K)+.918207*A1(K)^4 - .756704*A1(K)^5 + .482199*A1(K)^6
9070 GAMMA(K)=GAMMA(K)-.193528*A1(K)^7 + .035868*A1(K)^8
9080 GAMMA(K)=GAMMA(K)/A1(K)
9090 RETURN
9200 'SUBROUTINE BASELINE
9210 'THIS SUBROUTINE GENERATES THE PARABOLIC BASELINE FROM THE THREE
9220 'POINTS ENTERED IN THE D-S ANALYSIS SECTION
9230 M3=(XB(3)-XB(1))*(XB(2)-XB(1))
9240 M4=(XB(2)-XB(1))*(XB(3)-XB(2))
9250 M5=(XB(3)-XB(1))*(XB(3)-XB(2))
9260 AA=(XB(3)*XB(2)*YB(1)/M3)-(XB(3)*XB(1)*YB(2)/M4)+(XB(2)*XB(1)*YB(3)/M5)
9270 BB=-(XB(3)+XB(2))*YB(1)/M3 + (XB(3)+XB(1))*YB(2)/M4-(XB(1)+XB(2))*YB(3)/M5
9280 CC=YB(1)/M3 - YB(2)/M4 + YB(3)/M5
9290 FOR J% = 1 TO 256
9300 F(1,J%)=AA + BB*J% + CC*J%^2
9310 NEXT J%
9320 RETURN
```

B.2 MONTE CARLO SIMULATION PROGRAM

This program was written to simulate TiO_x island growth on a (111) or (100) surface. It was written for a Commodore 8032 personal computer equipped with visual memory. The program is composed of several steps:

(1) Displaying an N x N grid

(2) Randomly choosing nucleation sites (at a user-specified density)

(3) Randomly growing islands around these sites to coverages at 0.05 ML intervals

(4) Counting of sites (of a particular type)

Several programs of this form were written so as to count each type of site (*e.g.*, peripheral, adjacent-to-peripheral). Typically 100 x 100 "hexagonal" (~(111) surface) grids were employed with a nucleation site density of 4.5 x 10^{13} cm^{-2}. Due to the extraordinary amount of time required to execute this program, a column of dots to the right of the grid will appear to indicate the current row at which counting is occurring and to reassure the user that the program is indeed running.

```
1 DIM X(500),Y(500),RF(50),RR(50),RN(50)
2 PRINT"":CLEAR:F=0
3 PRINT"                    NEAR-PERIPHERY SITE COUNTING (W/ PLOT)":PRINT"":PRINT""
4 PRINT"CONTINUOUS MODE (Y OR N)":INPUT F1$:IF F1$="Y" THEN F=1
5 PRINT"NEAR-PERIPHERAL CALCULATION (Y OR N)?":INPUT F2$
6 IF F2$="Y" THEN F2=1
7 PRINT"ENTER LATTICE TYPE (S=SQUARE OR H=HEXAGONAL)"
8 INPUT LA$:IF LA$="S" OR LA$="H" GOTO 10
9 GOTO 7
10 PRINT"ENTER GRID SIZE (X,Y)":INPUT NX,NY
12 PRINT"ENTER NUCLEATION SITE DENSITY":INPUT N
1[illegible] PRINT"ENTER INITIAL [illegible] COVERAGE":INPUT THETA
1[illegible] IF F=1 THEN PRINT"ENTER FINAL [illegible] COVERAGE":INPUT TF
1[illegible] PRINT"ENTER RANDOM NUMBER SEED":INPUT SF:U=RND(SF)
2[illegible] [illegible]:PRINT""
25 CLS-R:POKE49151,3:OUTL1,1
30 FOR J=1 TO NY
3[illegible] LINE 10[illegible],2*J,2*NX+100,2*J
4[illegible] NEXT
6[illegible] N%=N*1.6E15*(NX*NY)
7[illegible] MOVE 100,190:AUTEXT "SEEDING: N=":AUTEXT STR$(N%)
75 AUTEXT "1":STR$(N):" SITES/CM2 "
80 FOR I=1 TO N%
90 U1=RND(1):V1=RND(1)
100 [illegible]:I1=2*U%+102:J1=2*V%+2
11[illegible] MOVE I1,J1:RDPIX VAR:IF VAR=2 THEN I=I-1:GOTO 120
11[illegible] WRF1:X(I)=I1:Y(I)=J1
11[illegible] [illegible]
1[illegible] NEXT
1[illegible] IF [illegible] N% THEN PRINT"SEED MISMATCH":STOP
1[illegible] [illegible]
1[illegible] M1=[illegible]
1[illegible] [illegible](NX*NY)
1[illegible] MOVE [illegible]:AUTEXT "ISLAND GROWTH:"
1[illegible] MOVE [illegible]:AUTEXT"COVERAGE="
1[illegible] MOVE [illegible]:AUTEXT STR$([illegible])
1[illegible] [illegible]:MOVE 16[illegible],1[illegible]:AUTEXT STR$(CO)
[illegible] IF [illegible] THEN GOTO 170
1[illegible] U1=RND(1):V1=RND(1)
1[illegible] [illegible]=2*U%+10[illegible]:V%=2*V%+2
1[illegible] MOVE U%,V%:RDPIX VAR:IF VAR[illegible] GOTO 135
1[illegible] FOR [illegible]
14[illegible] FOR [illegible]=1 TO [illegible]
14[illegible] I1=U%+[illegible]:J1=V%+[illegible]
14[illegible] IF I1 [illegible] THEN I1=I1+[illegible]*NX
14[illegible] IF I1 [illegible]*NX+100 THEN I1=I1-2*NX
15[illegible] IF J1 [illegible] THEN J1=J1+[illegible]*NY
15[illegible] IF J1 [illegible] THEN J1=J1-[illegible]*NY
1[illegible] MOVE I1,J1:RDPIX VAR
1[illegible] IF VAR[illegible] THEN M1=M1+1:MOVE U%,V%:WRF1:CO=M1/(NY*NX):GOTO 130
1[illegible] NEXT
1[illegible] NEXT
1[illegible] GOTO 135
1[illegible] MOVE 100,1[illegible]:AUTEXT"PERIPHERAL COUNTING:"
18[illegible] R[illegible]:F1=0:F[illegible]
1[illegible] SUM[illegible]
2[illegible] FOR J=1 TO NY:J1=2*J
2[illegible] FOR I1=1 TO NX:I1=2*I1+10[illegible]
2[illegible] MOVE I1,J1:RDPIX VAR:IF VAR[illegible] GOTO 250
21[illegible] SUM=0
2[illegible] FOR [illegible]=1 TO 3:L[illegible]=I1+2*([illegible]-2)
2[illegible] FOR [illegible]=1 TO 3:L[illegible]=J1+2*([illegible]-2)
2[illegible] IF LA$="H" AND L[illegible]=0 GOTO 235
2[illegible] IF [illegible] THEN [illegible]*NX
2[illegible] IF [illegible]*NX+100 THEN [illegible]-2*NX
2[illegible] IF [illegible] THEN L2=L2+2*NY
2[illegible] IF [illegible] THEN L2=L2-2*NY
2[illegible] MOVE [illegible]:RDPIX VAR:SUM=SUM+VAR
2[illegible] NEXT [illegible]
2[illegible] NEXT [illegible]
2[illegible] IF SUM [illegible] AND LA$="H" THEN R1=R1+1:GOTO 25[illegible]
2[illegible] IF SUM [illegible] AND LA$="S" THEN R1=R1+1:GOTO 25[illegible]
2[illegible] [illegible]:IF F[illegible]1 THEN GOSUB 400
250 NEXT I1
2[illegible] MOVE [illegible]:WRF1
2[illegible] NEXT J
2[illegible] [illegible](NX*NY)
2[illegible] [illegible](NX*NY)
2[illegible] [illegible]=RC:RN([illegible])=R[illegible]/(NX*NY)
2[illegible] MOVE 110,15[illegible]:AUTEXT"UNAFFECTED AREA=":
2[illegible] MOVE [illegible],15[illegible]:AUTEXT STR$(RC[illegible])
2[illegible] MOVE 110,14[illegible]:AUTEXT"PERIPHERAL AREA=":
2[illegible] MOVE [illegible],14[illegible]:AUTEXT STR$(F[illegible])
[illegible] IF F=1 THEN PRINT THETA,RF([illegible]),:PRINT RF([illegible]),RN([illegible])
[illegible] IF F[illegible]1 THEN PRINT THETA,RF([illegible]):PRINT RF([illegible])
3[illegible] IF F[illegible]1 GOTO 31[illegible]
30[illegible] THETA=THETA+0.05:IF TF[illegible]THETA THEN GOSUB 500:STOP
31[illegible] GOTO [illegible]
31[illegible] PRINT"SIMULATION COMPLETED"
3[illegible] PRINT"NEW COVERAGE? (Y OR N)"
3[illegible] INPUT A$
3[illegible] IF A$="N" THEN STOP
34[illegible] PRINT"ENTER NEW COVERAGE"
345 INPUT THETA
350 PRINT""
```

```
355 MOVE 110,150:AUTEXT"UNAFFECTED AREA=":
360 MOVE 205,150:AUTEXT STR$(RC0)
365 MOVE 110,140:AUTEXT"PERIPHERAL AREA=":
370 MOVE 205,140:AUTEXT STR$(RC0)
375 MOVE 110,1[illegible]:AUTEXT"PERIPHERAL COUNTING:"
380 GOTO 130
400 FOR L1=1 TO 5:L2=J1+2*(L1-3)
405 FOR I1=1 TO 5:I2=I1+2*(I1-3)
410 IF ABS(L1-3)[illegible]2 AND ABS(I1-3)[illegible]2 GOTO 430
415 IF [illegible] GOTO 435
420 IF I1+L1[illegible]4 OR I1+L1[illegible]8 GOTO 430
425 IF I2[illegible] THEN I2=I2+N
426 IF I2[illegible]N+1[illegible] THEN I2=I2-2*N
427 IF L2[illegible]2 THEN L2=L2+2*N
428 IF L2[illegible]2*N THEN L2=L2-2*N
429 MOVE [illegible]:READ VAR:IF VAR=2 THEN R2=R2+1:RETURN
430 NEXT I1
435 NEXT L1
440 RETURN
500 CLEAR
505 [illegible] 1,0:LINE 102,30,202,30
5[illegible] [illegible]
510 LINE 102,30,102,130
515 MOVE 115,20:AUTEXT"0.2":MOVE 135,20:AUTEXT"0.4"
51[illegible] MOVE 155,20:AUTEXT"0.6":MOVE 175,20:AUTEXT"0.8"
51[illegible] MOVE 195,20:AUTEXT"1.0":MOVE 130,10:AUTEXT"TIOX COVERAGE"
5[illegible] MOVE 72,40:AUTEXT"0.2":MOVE 72,60:AUTEXT"0.4"
5[illegible] MOVE 72,80:AUTEXT"0.6":MOVE 72,100:AUTEXT"0.8"
5[illegible] MOVE 72,120:AUTEXT"1.0"
5[illegible] FOR I[illegible]
5[illegible] THETA=THETA+0.05
5[illegible] PRINT"COVERAGE=",THETA
5[illegible] PRINT"ENTER RH[illegible]":INPUT R1
5[illegible] T1=THETA*100+10[illegible]
5[illegible] [illegible]*1000+30:MOVE T1,D:WRFI[illegible]
5[illegible] NEXT [illegible]
5[illegible] RETURN
```

U.S. DEPARTMENT OF COMMERCE
Technology Administration
National Technical Information Service
Springfield, VA 22161 (703) 605-6000